Department für Biomedizinische Wissenschaften
der veterinärmedizinischen Universität Wien

Institut für Physiologie, Pathophysiologie und Biophysik
Abteilung für Physiologie und Biophysik

# Investigation of gene and protein expression of uncoupling protein 4 in mouse brain under different dietetic conditions

Diplomarbeit
Zur Erreichung des akademischen Grades
Magister Medicinae Veterinariae

an der
Veterinärmedizinischen Universität Wien

vorgelegt von
Theresa Hommel

Wien, im Oktober 2021

Supervisors: Dr.rer.nat. Felix Locker
Univ.-Prof. Dr.med. Elena E. Pohl

Reviewer: Dipl.-Biol. Dr.rer.nat. Catharina Duvigneau

## Acknowledgements

I would like to thank everyone without whom this thesis could not have been completed:

First of all, I would like to thank my supervisor, Univ.-prof. Dr. med. Elena E. Pohl, for giving me the opportunity to conduct my thesis in her group and for providing helpful comments and suggestions.

I would also like to thank my second supervisor, Dr. rer. nat Felix Locker, who taught me the basics, supported me throughout the whole project, and even gave me the opportunity to learn so much that goes beyond this thesis.

I want to thank Dipl.-Biol. Dr. rer. nat. Catharina Duvigneau for the review of my thesis and the extensive and constructive feedback I received.

I would further like to express my sincere gratitude to MSc. Sarah Bardakji, Dipl.-Ing. Dr.rer.nat. Soleman Sasgary, and Bakk.rer.nat. Martin Hofer for their useful advice as well as technical support whenever I needed it.

I am grateful to the entire biophysics team, who welcomed me ever so warmly.

Last but not least, I would like to thank Julia Greiler, my great fellow student, with whom I could share all the ups and downs that I faced throughout this project, as well as my friends and family, who supported me emotionally and showed understanding when I did not have as much time for them as I would have wished.

# Table of content

# 1. Introduction

## 1.1 Uncoupling protein 4

### 1.1.1 Uncoupling proteins

Uncoupling protein 4 (UCP4) belongs to the subfamily of uncoupling proteins (UCPs), which in turn are classified as mitochondrial solute carrier proteins SLC25 (Palmieri 2004). They are located in the inner mitochondrial membrane (IMM).

UCP4 (SLC25A27) was originally found and assigned to the subfamily of UCPs due to its homology (~30%) to UCP2 and UCP3. The fact that UCP4 shares 39 conserved residues and eight conserved charges with this subfamily (Jezek 2000), referred to as unique uncoupling protein signature sequence, justifies its classification as UCP, even though phylogenetic analysis revealed closer relationships to oxoglutarate and dicarboxylate carriers (Borecky et al. 2001).

UCP1, formerly known as thermogenin, was the first discovered protein of this family. It is associated with the non-shivering thermogenesis in brown adipose tissue (BAT) through uncoupling processes (Nedergaard et al. 2001). Uncoupling is described as the process of dissipating the proton gradient, due to $H^+$ backflow across the IMM that leads to heat production instead of phosphorylation of ADP (Yu et al. 2000, Jezek et al. 2004). Other members of the uncoupling protein family were identified due to their homology to UCP1 using cDNA screening. However, UCP1 is the only member of this family which produces a substantial amount of heat (Pohl et al. 2019). The function of the other UCPs (2-5), as well as their distribution, is controversially discussed. For UCP2 and UCP3 an involvement in metabolic processes is proposed (Rupprecht et al. 2012, Pohl et al. 2019). This can be confirmed, in part, by the findings that UCP2 and UCP3 expression coincides with a distinct type of bioenergetic profile and protein markers. For example, in the developing heart there is a shift toward an increase in FAO (fatty acid oxidation) while at the same time the amount of UCP3 protein increases and UCP2 decreases (Hilse et al. 2018)(Fig. 1.1).

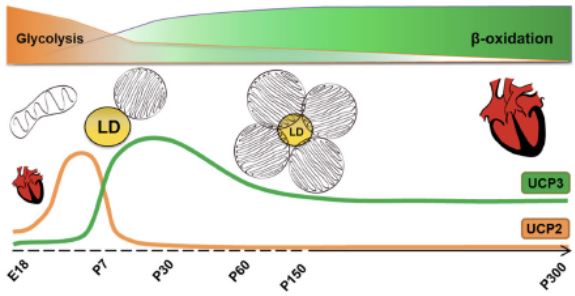


***Figure 1.1: UCP expression coincides with the bioenergetic profile of a cell.***
*The figure is taken from Hilse et al. 2018. LD-lipid droplet, E18-embryonal day 18, P7-postnatal day 7*

### 1.1.2 Distribution of UCP4

UCP4 is abundant to the central nervous system, where it is expressed especially in neurons but also in neurosensory cells (Smorodchenko et al. 2011), astrocytes (Smorodchenko et al. 2009), and oligodendrocytes (Liu et al. 2006).

UCP4 is present in fetal and adult tissues. Its amount increases during development from embryonic to postnatal stages (Smorodchenko et al. 2009).

Apart from UCP4 also UCP2 (Richard et al. 1998) and UCP5 (Sanchis et al. 1998) mRNA have been detected in the brain, which at this time was surprising, suggesting a similar function and homogeneous distribution. In the meantime, a new concept for the tissue distribution of UCP2 was proposed. It was shown to be abundant in proliferating cells like immune, stem, or cancer cells (Rupprecht et al. 2012, Rupprecht et al. 2014). Therefore, UCP2 gene and protein expression in brain can be assigned to the microglia, which are specialized immune effector cells of the central nervous system related to the monocyte macrophage lineage (Smorodchenko et al. 2017). UCP5 is assumed to differ from UCP4 in the regional distribution (Ramsden et al. 2012) since the UCP4 expression varies in different brain regions (Smorodchenko et al. 2009, Liu et al. 2006). However, Pohl group did not found UCP5 protein at all in brain using specific, validated antibodies (Smorodchenko et al. 2009, Smorodchenko et al. 2017).

### 1.1.3 Proposed functions of UCP4

Up to now, there are no knock-out models of UCP4 available and the high homology within the SLC25 transporter family and the resulting cross-reactivity of antibodies complicates research.

The physiological function of UCP4 is still not clear, although its neuroprotective role by participation in reactive oxidative species (ROS) regulation (Ramsden et al. 2012, Liu et al. 2006), thermogenesis (Yu et al. 2000) and calcium homeostasis (Liu et al. 2006) was proposed, based on its homology to UCP1 and putative proton transport function. Indeed, the very long lifetime of UCP4 protein (unpublished results) and expression pattern during mammalian development (Smorodchenko et al. 2009) does not support its involvement in non-shivering thermogenesis, described for UCP1.

Previous studies have suggested that UCP4 increases resistance against oxidative stress. Expression of UCP4 in pheochromocytoma cells led to a significantly lower respiration control rate, representing a higher uncoupling activity, than the control cells. This lowers the generation of ROS. Furthermore, the same study observed increased $Ca^{2+}$ concentrations and decreased neuronal survival in UCP4 deficient hippocampal neuron cultures (Liu et al. 2006).
However, results of Pohl et al. have not shown the change of UCP4 abundance under increased ROS amounts or hypoxia (Smorodchenko et al. 2011).

In experiments with FCCP, resulting in uncoupling of mitochondrial oxidation, UCP4 expressing cells maintained a significantly higher level of ATP than control cells. This indicates compensation through an alternative pathway of ATP production in UCP4 expressing cells (Liu et al. 2006). Besides that, also glucose uptake and lactate levels of these cells were significantly higher. These results suggest that UCP4 may promote a metabolic shift towards glycolysis (Liu et al. 2006) which in turn reduces ROS generation even further.
The metabolic shift was also observed for astrocytes in vitro, where UCP4 overexpression after transfection with UCP4 lentiviral constructs increased glucose uptake and lactate release as well, indicating increased anerobic glycolysis, while the efficiency of OXPHOS was reduced (Perreten Lambert et al. 2014). In this case, the decreased efficiency of OXPHOS was caused by mitochondrial acidification which was shown to be a result of UCP4 expression (Perreten Lambert et al. 2014). At this point, the question arises to what extent this lactate metabolism-associated role in astrocytes is important, despite the extremely low abundance of UCP4 in astrocytes compared to neurons.
Another study (Sullivan et al. 2004) has reported that a ketogenic diet (KD) increases UCP4 but also UCP2 and UCP5 expression in the brain, which goes along with increased uncoupling activity in their experiments. However, the value of these experiments is

questioned because no evidence for the specificity of the antibodies used for the uncoupling proteins were presented.

Since recent results of Pohl group imply that protein expression of UCP4 family members (UCP2 and UCP3) coincide with distinct metabolic conditions and they have a metabolic function as dual transporters for protons and substrates, further investigation of UCP4 expression under different metabolic conditions might be interesting.

## 1.2 Mitochondria play a central role in metabolism

### 1.2.1 Energy production in mitochondria

To further understand the energy supply and possible interactions with UCP4 we should have a closer look on mitochondria, where the energy production takes place. Mitochondria are therefore also commonly called „the powerhouse of the cell“. 30-32 molecules of ATP, which is the most important versatile energy carrier (Alberts et al. 2002), are generated during oxidative phosphorylation (OXPHOS) at the inner mitochondrial membrane. The electron transport chain (ETC) includes four respiratory chain complexes and ATP synthase (Alberts et al. 2002). NADH and $FADH_2$ generated in the TCA cycle, in which pyruvate as an end product of glycolysis, fatty acids (FA) and ketone bodies can be incorporated after conversion to acetyl-CoA, donate electrons either to complex I (ubiquinone oxidoreductase) or complex II (succinate dehydrogenase) (Nolfi-Donegan et al. 2020). These electrons are transported along with the ETC whereby protons are pumped from the mitochondrial matrix into the mitochondrial intermembrane space at complexes I, III, and IV. Finally, these electrons are transferred to molecular oxygen which is thereby reduced to water. This process results in the generation of a protonmotive force due to the proton concentration and electrochemical gradient, which leads to reentry of $H^+$ to the mitochondrial matrix through ATP synthase, coupled to the production of ATP from ADP (Nolfi-Donegan et al. 2020).

The activity of cellular respiration, as well as the fuel, is tissue-dependent. Because of their high energy demands, mitochondrial disorders are most prevalent in tissues like the brain, the heart, or the endocrine system (Wallace et al. 2010). In the brain, mitochondrial dysfunction is considered to be a pathological key process of neurodegenerative disorders like epilepsy, multiple sclerosis, and others (Wu et al. 2019).

### 1.2.2 Mitochondria support metabolic plasticity

In addition to their function as energy producers, mitochondria play a vital role in metabolic plasticity. This plasticity is enormously important in the brain to maintain a constant energy supply to protect vital functions.

Depending on substrate abundance, in several tissues, a shift either towards glycolysis, or fatty acid oxidation (Wallace et al. 2010) or ketogenesis is induced. Here, ketogenesis is proportional to total fat oxidation in the liver (Puchalska and Crawford 2017). High amounts of glucose stimulate insulin secretion, which in the end suppresses peroxisome proliferator–activated receptor gamma coactivator 1 alpha (PGC1a) expression leading to downregulation of OXPHOS and antioxidant defense. Analogously a lack of carbohydrates increases PGC1a transcription (Wallace et al. 2010). Besides that, decreased glycolysis leads to a low $NADH/NAD^+$ ratio in the cytoplasm. This stimulates sirtuin 1 (SIRT1) catalysing $NAD^+$ - dependent deacetylation of PGC1a (Lagouge et al. 2006), resulting in the promotion of mitochondrial biogenesis and metabolic adaptation (Ventura-Clapier et al. 2008)(Fig. 1.2).

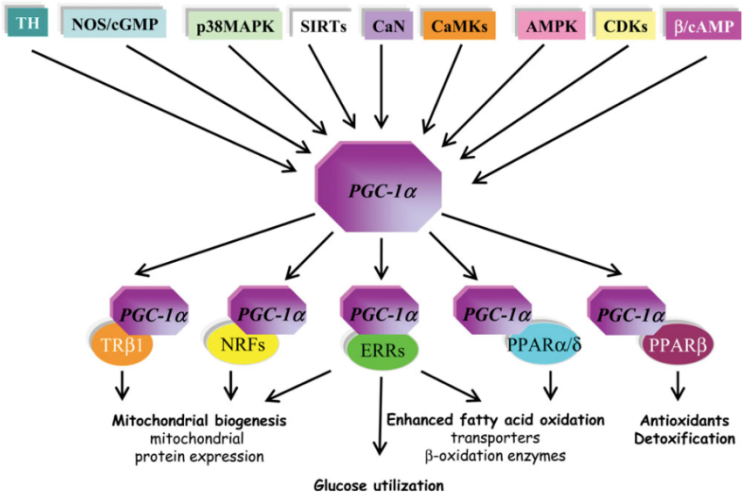


***Figure 1.2: PGC1a a key regulator in mitochondrial metabolism***
*The figure is taken from Ventura-Clapier et al. 2008*
*TH-Thyroid hormone, NOS/cGMP-nitric oxide synthase, p38MAPK-p38 mitogen-activated protein kinase, SIRT-sirtuine, CaMKs-calcineurin, calcium-calmodulin-activated kinases, AMPK-adenosine-monophosphate-activated kinase, CDKs-cyclin-dependent kinase, b/cAMP-b-adrenergic stimulation, PGC1a-peroxisome proliferator–activated receptor gamma coactivator 1 alpha, TRß1-thyroid hormone receptor-ß1, NRF-nuclear respiratory factor, ERR-estrogen-related receptors, PPAR-peroxisome proliferator-activated receptors*

However, mitochondria in the brain are more limited in terms of their substrate, as a lot of energy has to be provided in a very short time (Schönfeld and Reiser 2013).

## 1.3 Energy supply in the brain

Although the brain has just a proportion of 2% of total body weight in humans and rodents and even less in other mammals, in humans it requires about 20% of the body's total energy expenditure in the basal metabolic state (Rolfe and Brown 1997, Jensen et al. 2020). Since most mitochondria are found in the dendrites and synaptic terminals, the metabolic rate is 25-50% higher in the gray matter, where the neurons are located, than in the white matter (Rolfe and Brown 1997). However, energy is not only needed during the generation of action potentials or pre- and postsynaptic events but also for so-called „housekeeping processes", such as actin cytoskeleton remodeling or axonal transport (Bordone et al. 2019).

Apart from the neurons, the brain consists of five other different cell types, astrocytes, microglia, oligodendrocytes, ependymal cells, and endothelial cells which all have different energy demands.
Neurons are specialized cells for the transmission and progressing of signals derived from neurosensory cells. Astrocytes belong to the group of glial cells. They are major players in the formation of the neurovascular unit (Bell et al. 2020) and have multiple functions. In this context most important might be the formation of the blood-brain barrier together with endothelial cells and uptake of energy substrates from the blood, as well as the supply of energy to neurons (Takahashi 2020). The group of glial cells also includes oligodendrocytes, which form the myelin sheaths of the central nervous system, and microglia, which are responsible for the immune defense. Ependymal cells are specialized epithelial cells, which line the cavities in the brain like ventricles or the spinal cord's central canal (Rodler and Sinowatz 2019).

Especially neurons are known for their close dependence on astrocytes concerning their energy supply. Under physiological conditions, meaning a sufficient amount of metabolizable glucose, which is the main energy source in the brain (Magistretti and Allaman 2015), astrocytes are predominantly glycolytic even under normoxic conditions. They release lactate which is further used by neurons in which OXPHOS predominates (Itoh et al. 2003, Schönfeld and Reiser 2013).
As shown in figure 1.3, glucose is taken up in the brain via glucose transporters, GLUT1 in astrocytes, and GLUT3 in neurons respectively (Takahashi 2020). Since the brain has almost no glucose storage, energy has to be provided continuously via the bloodstream (Takahashi 2020). Just astrocytes and possibly embryonic neurons can store a small amount of glycogen (Falkowska et al. 2015) and can provide energy as lactate or pyruvate under conditions of glucose shortage for a few minutes. These metabolites leave the astrocytes via

monocarboxylate transporters 1 and 4 and enter the neurons via monocarboxylate transporter 2, where they are incorporated into the Krebs cycle. Neuronal synaptic activity additionally stimulates glycolysis in astrocytes and donation of the metabolites (Schönfeld and Reiser 2013). Despite its function as a substrate, astrocytic lactate can also serve as a signaling molecule, increasing the blood flow to improve the supply of active brain areas (Schönfeld and Reiser 2013).

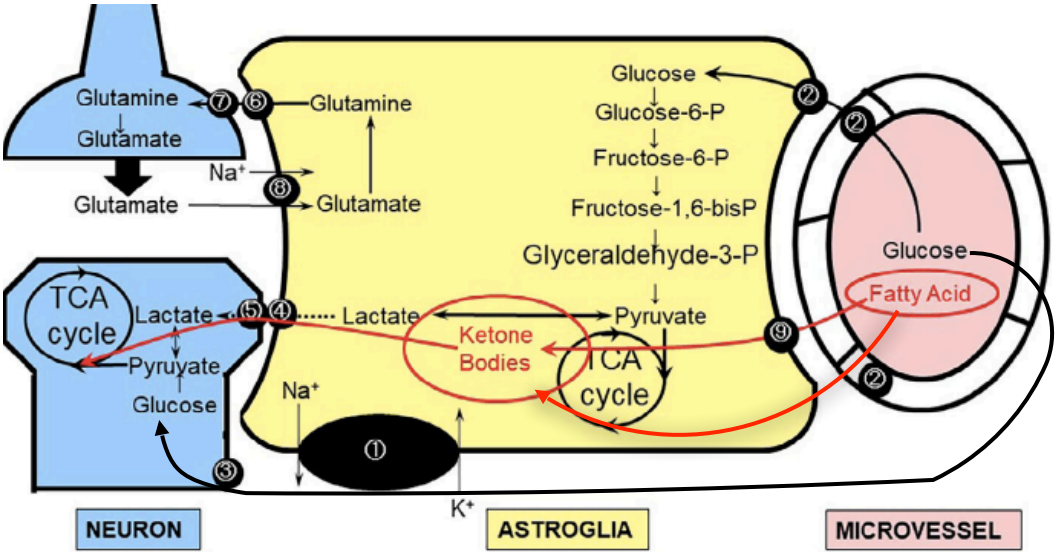


***Figure 1.3: neuron-astrocyte metabolic coupling***
*1) Na+,K+-ATPase, 2) glucose transporter 1, 3) glucose transporter 3, 4) monocarboxylate transporter1/4 (astrocytic), 5) monocarboxylate transporter 2 (neuronal). 9) fatty acid-binding protein (FABP). FAs are actively or passively taken up by astrocytes are converted into KBs which are transferred to the neurons via monocarboxylate transporters, where they can enter TCA-cycle. Glucose can be taken up by neurons directly or by astrocytes via GLUTs. Astrocytes metabolize glucose, and supply the neurons with lactate, transported by MCTs. TCA-tricarboxylic acid cycle.The figure is taken and adapted from Takahashi 2020.*
*TCA-tricarboxylic acid cycle*

Depending on the metabolic state of the organism, the brain is able to use different energy substrates. These include medium-chain fatty acids (MCFA) (Ebert et al. 2003, Edmond et al. 1987) and ketone bodies such as beta-hydroxybutyrate and acetoacetate (Owen et al. 1967). MCFA can pass the blood-brain barrier in contrast to long-chain fatty acids (LCFA), as great fractions of MCFAs are not bound to albumin in the blood or fatty acid-binding proteins in the cytoplasm (Schönfeld and Wojtczak 2016). Moreover, the transport of MCFA to mitochondria in their non-esterified form does not require the CPT1/CACT/CPT2 transport system, whereas the availability of LCFA depends on the activity of this transport system. Thereby, CPT1 converts the acetyl-CoA on the cytosolic side at the OMM, the resulting acylcarnitine is transported by CACT into the mitochondrion, and CPT2 reconverts acylcarnitines to acetyl-

CoA at the IMM (Ceccarelli et al. 2011, see Fig. 3.10) Furthermore, the usage of LCFA is limited due to a lower enzymatic capacity in brain than other tissues that require large amounts of energy (Schönfeld and Reiser 2013). MCFAs are activated by medium-chain acyl-CoA synthetase in the mitochondrial matrix and used as substrates for ß-oxidation and TCA-cycle (Schönfeld and Wojtczak 2016). Additionally, octanoate (C8) stimulates ketogenesis and thereby release of ß-hydroxybutyrate in astrocytes (Thevenet et al. 2016). Although astrocytes are capable to synthesize and provide ketone bodies themselves (Takahashi et al. 2014), the greatest proportion of ketone bodies originates from the liver and enter the brain via monocarboxylate transporter 1 and 4 and neurons via monocarboxylate transporter 2 (Takahashi 2020) thus the same monocarboxylate transporters as needed for lactate and pyruvate shuttle (Bordone et al. 2019).

A major advantage of ketone bodies in contrast to pyruvate or lactate is that activity of rate-limiting enzyme pyruvate dehydrogenase complex (PDHC) is not required for conversion into acetyl-CoA, before entering the TCA cycle (Takahashi 2020). This is particularly important in hypoxic conditions, for example after ischemic brain injury, since PDHC is highly susceptible to oxidative stress (Martin et al. 2005, Takahashi 2020).

Although LCFAs could provide about twice as much energy than glucose, less than one-quarter of the required ATP is generated by ß-oxidation of LCFA and is practically limited to astrocytes (Schönfeld and Reiser 2013). One of the reasons could be the higher oxygen consumption of this pathway and thereby a higher risk of hypoxia (Schönfeld and Reiser 2013). Furthermore, non-esterified fatty acids (NEFA) could lead to depolarization of the IMM and enhanced generation of ROS. Since ketone bodies do not have these adverse properties, they are a very suitable and preferred substrate to compensate for a glucose deficiency in brain (Schönfeld and Reiser 2013).

## 1.4 Impact of diets on metabolism

### 1.4.1 Ketogenic diets (KDs)

Due to the positive effects on the brain, KDs were introduced in the 1920s as an alternative treatment option for epilepsy (for review see Kossoff and Wang 2013). They were originally designed to mimic the effects of starvation over longer periods and consist of high-fat, adequate protein and in contrast to high-fat diets low-carbohydrate amounts. While in the first years extreme versions of KD with severe adverse effects (Wheless 2001) were used, today a “well-formulated“ KD, characterized by a less reduced total carbohydrate and protein intake, which increases ketone bodies only to a range of nutritional ketosis (Miller et al. 2018) is established. Interestingly, KDs were shown to increase the health- and life-span in mice

(Roberts et al. 2017), which is in line with experiments on the positive effects of caloric restriction in rodents (Lin et al. 2014).

There are two different options to accomplish the state of nutritional ketosis without fasting (Fig. 1.4). First through ingestion of MCFA like C8, which stimulates ketogenesis in astrocytes and in the liver and leads to endogenous ketones; and second the supplement of exogenous ketone esters and salts to the diet (Jensen et al. 2020). The largest amount of ketone bodies during KD is produced in the liver by FA oxidation, where methylglutaryl-CoA synthase 2 (HMGCS2) is required as the rate-limiting enzyme. These ketones, ß-hydroxybutyrate (BHB), acetoacetate, and acetone, are transported via the blood without being bound to plasma proteins. In the brain, up to 60% of energy requirements can be covered by ketone bodies (Miller et al. 2018). Furthermore, BHB is considered to act as a signaling molecule, for example in inhibiting insulin-mediated glucose uptake, mTOR pathway or autophagy (Rojas-Morales et al. 2016)

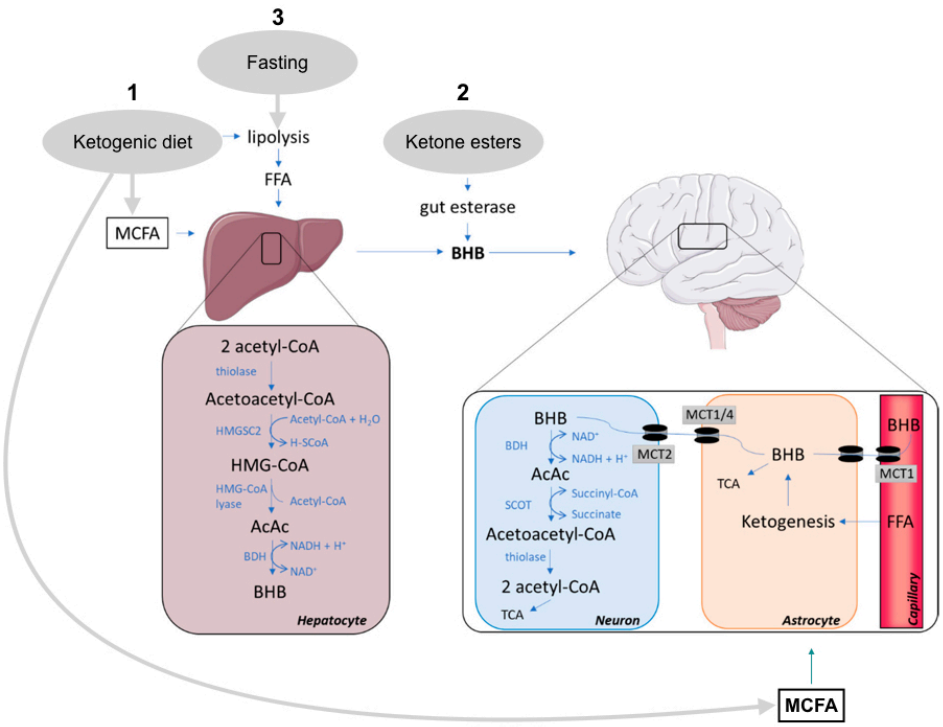


***Figure 1.4: Production and usage of ketone bodies***

*Nutritional ketosis can be accomplished by 1) ingestion of MCFA, 2) exogenous ketone esters or 3) fasting. The figure is taken and modified from Jensen et al. 2020.*

*FFA-free fatty acids,MCFA-medium chain fatty acids, TCA-tricarboxylic acid cycle, BHB-ß-hydroxybutyrate, AcAc-acetoacetate MCT-monocarboxylate transporter, BHD-ß-hydroxybutyrate dehydrogenase, HMG-CoA -3-hydroxy-3-methylglutaryl-CoA, HMGCS2-3-Hydroxy-3-Methylglutaryl-CoA synthase 2, SCOT-succinyl-CoA:3-ketoacid coenzyme A transferase*

### 1.4.2 Fasting conditions

Fasting conditions like calorie restriction (CR) and intermittent fasting (IF) are popular methods to lose weight and improve general health. Fasting causes depletion of the cells' glycogen stores after a certain period of time. This leads to the metabolization of lipids from adipocytes to fatty acids to use them as an energy substrate and results in ketogenesis (Anton et al. 2018, Longo and Mattson 2014). The latter is more pronounced in IF (Martin, Mattson and Maudsley 2006). Less availability of glucose on one hand protects from protein damage due to non-enzymatic glycation. The same glucose utilization rate of fasted and *ad libitum* fed mice, although they had different plasma glucose and insulin levels, on the other hand also indicates improved glucose effectiveness, insulin responsiveness, or both (Martin, Mattson and Maudsley 2006).

Caloric restriction has been shown to elevate the capacity of OXPHOS and preserve metabolism in aging. Thus it prevents age-related decline of neuronal activity in rats and increases live-span (Lin et al. 2014). Furthermore, it is reported that caloric restriction decreases body temperature, increases insulin sensitivity, and reduces mitochondrial oxidative stress (Mattson 2003). Similar to CR, IF displayed positive effects on several cardiovascular and neuronal risk factors, insulin sensitivity, and mitochondrial function (Anton et al. 2018).

## 1.5 Hypothesis

In the present work, we hypothesized that UCP4 is crucial for neuronal adaptation to different nutrient availability in mice brain, and therefore its gene and protein expression levels in neurons will differ compared to the standard diet fed mice accordingly. Furthermore, we hypothesized that UCP4 gene and protein expression patterns differ throughout the brain of mice given the different anatomical structure and metabolic demands of neurons in the specific brain regions.

## 1.6 Aim of the study

The aim of this diploma thesis was to determine, (i) whether UCP4 expression at gene and protein levels in the murine brain correlates with the change of energy substrate usage induced by dietary interventions like

1. KDs (consisting of either just long chain triglycerides (LCT) or a mixture of LCT and medium chain triglycerides (MCT)
2. fasting conditions (CR and IF)

and if there is a correlation to other metabolic markers. We analyzed gene expression in hypothalamus, hippocampus, cerebellum and „restbrain“ for glucose transporter 3 (Glut3) and glucokinase (Gck),and the FA importing acyl-carnitine system (CACT, CPT1c, CPT2) and lipid handling protein perilipin 3 (PLIN3). Furthermore, we analyzed expression of cytoplasmatic superoxide dismutase 1 (SOD1) as a marker for oxidative stress and PGC1a to see whether mitochondrial biogenesis is stimulated by the diets. Additionally, we checked UCP4 protein expression within the different diets with Western Blot.

Using immunoblot, we further aimed to determine, (ii) whether UCP4 protein amount differs regionally in the brain.

# 2. Materials and Methods

## 2.1 Materials

### 2.1.1 Mice and Diets

(i)40 and (ii)15 male C57/Bl6NRJ mice were used for the experiments in the animal facility of our cooperation partner (Kalina Duszka, University of Vienna).

***Table 2.1**: Diets*

| Diet | Product number | Company |
|---|---|---|
| Standard Diet (SD) | S9139-E028 | ssniff |
| LCT | S9139-E025 | ssniff |
| LCT/MCT | S9139-E032 | ssniff |
| IF | V153x R/M-H auto | ssniff |
| KR | V153x R/M-H auto | ssniff |

### 2.1.2 Chemicals and Kits

Further standard laboratory equipment, plates, tubes, pipet tips of following companies was used: Roth (Austria), VWR (Austria), Eppendorf (Austria).

***Table 2.2**: Assay Kits*

| Kit | Product number | Company |
|---|---|---|
| innuSOLV RNA Reagent | 845-SB-2090100 | Analytik Jena, Germany |
| Lysing matrix D | 6913-500 | MP Biomedicals, Germany |
| Glycogen | R0561 | Thermo Fisher Scientific, Austria |
| RNA ScreenTape Assay | 5067(-5576, -5577, -5578) | Agilent, Austria |
| DNAse I, RNAse-free | EN0521 | Thermo Fisher Scientific, Austria |
| High-Capacity cDNA Reverse Transcription Kit | 4368814 | Thermo Fisher Scientific, Austria |

| | | |
|---|---|---|
| RiboLock RNase Inhibitor | EO0382 | Thermo Fisher Scientific, Austria |
| Luna | M3003E | New England Biolabs, Germany |
| SYBR Safe DNA Gel Stain | S33102 | Thermo Fisher Scientific, Austria |
| Bromophenolblue | 114391-5G | Sigma-Aldrich, Austria |
| 1kb Hyperladder | BIO-33025-BL | Bioline |
| 100bp Ladder | N3231S | New England Biolabs, Germany |
| BCA Protein Assay | 23227 | Thermo Fisher Scientific, Austria |
| Precision Plus Protein Dual Color Standard | 1610374 | BioRad, Germany |
| Clarity™ Western ECL Substrate | 1705061 | BioRad, Germany |
| Amersham™ Protran™ 0,45$\mu$m NC | 10600002 | GE Healthcare , Austria |
| Protease Inhibitor cocktail | P8340-5ML | Sigma-Aldrich, Austria |

***Table 2.3**: Chemicals*

| | Product number | Company |
|---|---|---|
| Ammoniumperoxodisulfat (APS) | 9592.3 | Roth, Austria |
| Boric acid | A3581 | Applichem, Germany |
| Bovine Serum Albumin (BSA) | A9647-50G | Sigma-Aldrich, Austria |
| Desoxycholic acid sodium salt (DOC) | 3484.2 | Roth, Austria |
| EDTA | 8043.2 | Roth, Austria |
| Glycerin | 3783.1 | Roth, Austria |
| Glycin | T873.2 | Roth, Austria |
| Isopropanol | 9866.1 | Roth, Austria |
| Methanol | 8388.1 | Roth, Austria |
| 2-Mercaproethanol | 4227.3 | Roth, Austria |

| | | |
|---|---|---|
| nf-$H_2O$ | E476-500ML | VWR, Austria |
| low fat powdered milk | T145.1 | Roth, Austria |
| Natriumcitrate | 4088.1 | Roth, Austria |
| Natriumchloride (NaCl) | 9265.1 | Roth, Austria |
| Ponceau S | 5938.2 | Roth, Austria |
| Rotiphorese GelA (Acrylamid) | 3037.1 | Roth, Austria |
| Rotiphorese GelB (Bisacrylamid) | 3039.1 | Roth, Austria |
| fuming hydrochloric acid | 4625.1 | Roth, Austria |
| SDS | 0183.3 | Roth, Austria |
| TEMED | A1148,0025 | Applichem, Germany |
| Thimerosal | 6389.1 | Roth, Austria |
| Tris | AE15.2 | Roth, Austria |
| Trichloroacetic acid | 3744.2 | Roth, Austria |
| Triton X-100 | 3051.3 | Roth, Austria |
| Tween20 | 9127.3 | Roth, Austria |

### 2.1.3 Primer

*Table 2.4 Primer*

| Primer | Accession number | Direction | Sequence 5'-3' | GC [%] | Tm [°C] | Amplicon length [bp] | Slope | Efficency | Company |
|---|---|---|---|---|---|---|---|---|---|
| **mRPL4** | NM_024212.4 | forward | GTATGGCACTTGGCGGAAGG | 60.00 | 61.4 | 124 | 3.5419 | 91.57 | Microsynth |
| | | reverse | TGCTCGGAGGGCTCTTTGG | 63.16 | 62.0 | | | | |
| **mUCP4** | NM_028711.4 | forward | GTGGCCGAGCTAGCAACCTT | 60.00 | 62.8 | 101 | 3.4 | 96.84 | Microsynth |
| | | reverse | GAGTCCACTGCGCCATCTCC | 65.00 | 62.9 | | | | |
| **mGlut3** | NM_011401.4 | forward | GGGACAACGAAGGTGACCCC | 65.00 | 62.7 | 180 | 3.53 | 91.99 | Microsynth |
| | | reverse | GGCAGTCAGCAGTCCCTCAC | 65.00 | 62.8 | | | | |
| **mMCT2** | NM_011391.2 | forward | GTCATCTGACAACAGCCAAGAGA | 60.56 | 47.8 | 72 | 3.52 | 92.35 | Microsynth |
| | | reverse | GAGCTCTTGCTTTGGGGGTTT | 47.83 | 52.4 | | | | |
| **mGck** | NM_001287386.1 | forward | AGCTGCTGCGGAACACTGAG | 60.00 | 63.1 | 117 | 3.653 | 87.82 | Microsynth |
| | | reverse | TGCCAGGATCTGCTCTACCTTT | 50.00 | 61.2 | | | | |
| **mCACT** | NM_020520.5 | forward | GCAGACGAGCCGAAACCCAT | 60.00 | 68.0 | 109 | 3.2078 | 104.99 | Microsynth |
| | | reverse | GTCGGACCTTGCCGTGTCC | 65.00 | 67.6 | | | | |
| **mCPT1c** | NM_001252470.1 | forward | GCGAGGTGTCTCTGGGTTTCA | 57.14 | 62.3 | 181 | 3.6164 | 89.02 | Microsynth |
| | | reverse | CCTGGGCCCCGGTCAGA | 76.47 | 63.3 | | | | |
| **mCPT2** | NM_009949.2 | forward | CCAGCTACATCTCAGGCCCC | 65.00 | 62.1 | 98 | 3.2858 | 101.53 | Microsynth |
| | | reverse | CGGGTCCGGATTGAATGCCA | 60.00 | 62.9 | | | | |
| **mPLIN3** | NM_025836.3 | forward | GTCAAGACCCTCACCACGGC | 65.00 | 63.1 | 83 | 3.3932 | 97.11 | Microsynth |
| | | reverse | TCACTGGCCGTCGCAATCTG | 60.00 | 63.1 | | | | |
| **mSOD1** | NM_011434.2 | forward | CGGCGGATGAAGAGAGGCAT | 60.00 | 62.4 | 71 | 3.2639 | 102.48 | Microsynth |
| | | reverse | CACATTGGCCACACCGTCCT | 60.00 | 63.0 | | | | |
| **mPGC1$\alpha$** | NM_008904.2 | forward | GCGTCATTCGGGAGCTGGAT | 60.00 | 62.7 | 83 | 3.3647 | 98.25 | Microsynth |
| | | reverse | CCAACCAGAGCAGCACACTCT | 57.14 | 62.6 | | | | |

In table 2.4 , the genes were designated, for example, as mUCP4 instead of UCP4, indicating the animal species mouse. In the text, both terms are used synonymously.

### 2.1.4 Antibodies

***Table 2.5:*** *primary antibodies*

| Antibody | Antibody type | Isotype | molecular weight of protein, kDa | Dilution | Secondary AB | Product number | Company |
|---|---|---|---|---|---|---|---|
| Anti-UCP4 | polyclonal | IgG | 36 | 1:5000 | Rabbit | selfmade | Pineda |
| Anti-VDAC | monoclonal | IgG2b | 31 | 1:5000 | Mouse | ab14734 | abcam |
| Anti-SDHA | monoclonal | IgG1 | 70 | 1:5000 | Mouse | ab14715 | abcam |
| Anti-OGDH | polyclonal | IgG | 116 | 1:5000 | Rabbit | 15212-1-AP | Proteintec |
| Anti-ßActin | monoclonal | IgG1 | 42 | 1:5000 | Mouse | A5441 | Sigma |
| Anti-GFAP | monoclonal | IgG | 50 | 1:1000 | Rabbit | 12389S | Cell signaling |
| Anti-NeuN | monoclonal | IgG1 | 46-48 | 1:1000 | Mouse | MAB377 | Millipore |
| Anti-IBA-1 | polyclonal | IgG | 17 | 1µg/ml | Goat | ab5076-100 | abcam |

***Table 2.6:*** *secondary antibodies*

| Antibody | Isotype | Dilution | Product number | Company |
|---|---|---|---|---|
| rabbit | IgG | 1:5000 | 7074S | Cell signaling |
| mouse | IgG | 1:5000 | NA931V | GE healthcare |
| goat | IgG | 1:5000 | HAF017 | R&D Systems |

## 2.2 Methods

### 2.2.1 Experimental setup

Mouse brain samples were obtained from our cooperation partner (Kalina Duszka, University of Vienna), who performed the animal experiments. All animal experiments have been approved by the national authority according to §§ 26ff. of Animal Experiments Act, Tierversuchsgesetz 2012-TVG 2012 (BMWFW-66.006/0008-V/3b/2018).

Two experiments using male C57/BL6NRJ mice were performed: (i) n=40 mice for 5 diets (2019) and (ii) n=15 mice for 3 different diets (2021). The standard environment of the animal facility was a 12h/12h dark-light cycle in a room with a temperature around 20°C. The first twelve weeks after birth, the mice were kept under the same dietary conditions. Afterwards they were divided in (i) five/ (ii) three groups with eight animals each. Each of these groups was put on one of the different diets (SD, LCT, LCT/MCT, CR, IF) over a time period of eight weeks.

The composition of the diets differed primarily in their proportion of carbohydrates and fat as shown in the figure 2.1 and in supplementary table 1. Both ketogenic diets (KDs) had an 8:1 ratio of fats to carbohydrates.

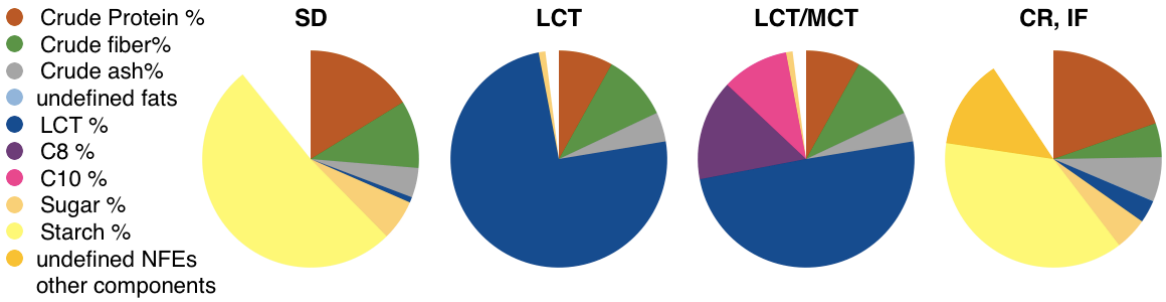


***Figure 2.1: Nutrient composition of diets***
*Ketogenic diets (LCT, LCT/MCT) differ from SD by their amount of crude fat, while fasting diets (CR,IF) differ primarily by the feeding regime, exact percentages of the nutrients are listed in the supplementary data.*
*SD-standard diet, LCT-long chain triglycerides, LCT/MCT-long and medium chain triglycerides, CR-caloric restriction, IF-intermitted fasting*

SD, LCT and LCT/MCT were offered ad libitum. CR and IF group received the same diet but in different quantities and at different time points. CR mice were fed once a day with an amount of 70% of regular diet while IF had ad libitum access for 24 h followed by a fasting period without any food for 24 hours. The day before euthanasia was a fasting day. Water was provided ad libitum in all of the groups.

Feeding trial was repeated for SD; LCT and LCT/MCT with 5 animals in each group in 2021 for statistic.
Prior to the main experiments, isolation method was tested with brain regions of 4 pre-test mice within the framework of TVG 2012 §2c „animal consumption“. Pre-test tissue was further used for validation of qPCR primers (see chapter 2.2.7)

### 2.2.2 Brain dissection

Mice were euthanized by an overdose of Isofluran® followed by cardiac puncture. The head was cut off and the skin pulled over the head in rostral direction. Cranial cavity was opened by cutting the skull with a small pair of scissors starting from the great foramen in the median plane up till an imaginary line between the eyes. Relief cuts are made on both sides, and the skullcap gently broke off with forceps. The brain was removed and directly put on a cooled plate on ice.
At first cerebellum was carefully separated without destroying the brainstem, afterwards brainstem was cut off. In the next step, a dorsal incision vertical to median plane was made slightly rostral of the middle of the median line. In both rostral quarters, cortex was carefully pulled away with two curved forceps until the striatum could be visualized, then they were pinched out. The brain was flipped to have the ventral side up and the hypothalamus can be removed. Then the brain was flipped back and the hippocampus was dissected along the entire length.
The remaining brain tissue, including cortex and different nuclei (see Fig.2.2), was collected and is in the following thesis referred to as „restbrain“.
All brain regions were directly transferred into Kryotubes and snap frozen in liquid nitrogen. They were stored at -80°C until further processing, restbrain was powdered in a mortar using dry ice and liquid nitrogen before storage.

***Table 2.7:*** *Brain regions*

| Tissue | amount, mg |
|---|---|
| Hypothalamus | ~ 5-10 |
| Hippocampus | ~ 15-20 |
| Cerebellum | ~ 30 |
| Restbrain (powdered) | ~ 300 |

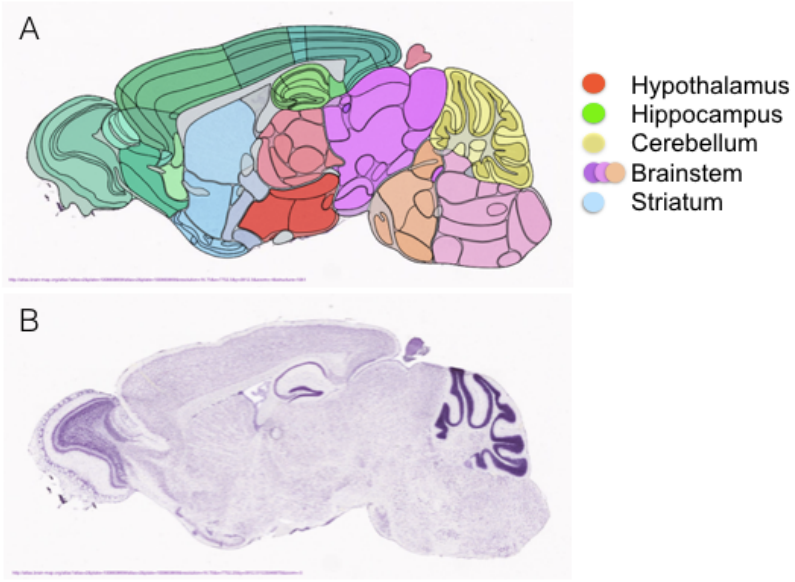


***Figure 2.2: Sagittal section through an adult mouse brain***
***A*** *schematic overview showing the division into distinct brain regions and* ***B*** *Nissl-stained histological image showing the distribution of neurons within these regions.*
*Pictures are taken from http://atlas.brain-map.org/atlas?atlas=2.*
*For this study, hypothalamus, hippocampus, striatum, cerebellum, and brainstem were taken separately. Remaining brain tissue, including cortex and olfactory bulb (dark green in schematic overview) and thalamus (light red), was pooled and labeled as restbrain.*

### 2.2.3 Sample preparation

RNA and protein were isolated with an optimized guanidine isothiocyanate/phenol-method using InnuSolv Reagent (Analytik Jena, Germany)
Because of the toxicity of InnuSolv Reagent, the whole procedure was performed under a fume hood.

First, 1 ml of the InnuSolv Reagent was pipetted in the pre-cooled Lysing matrices D (MP Biomedicals, Germany) and put on ice. Tissue was quickly transferred from the kryotube, stored on dry ice, into the lysing matrices with the reagent inside. Tissue was homogenized for 40 s using FastPrep-24 (MP Biomedicals, Germany) and the Quick-Prep Adapter.
The homogenates including the foam, which occurred through the homogenization step were transferred to 2 ml Eppendorf Tubes®.

Since restbrain was already powdered, two spatula tips of powder were directly transferred into a 2 ml Eppendorf Tube on dry ice and dissolved with 1 ml InnuSolv (Analytik Jena, Germany) by pipetting gently up and down.
Between the samples either forceps or spatula was cleaned with ethanol and distilled water to avoid contamination.
The samples were incubated at room temperature for 10 min. Afterwards 100 µl chloroform were added to every sample and the samples were shaken vigorously for 15 s until the appearance of the fluids changed from transparent to milky. After another incubation time of 10 min at room temperature, samples were centrifuged for 5 min at 12000xg and 4°C to obtain phase separation.
The upper, colorless phase (Fig. 2.3) consists of the dissolved RNA, the white interphase contains the DNA. The red phase at the bottom is the organic phase including proteins.

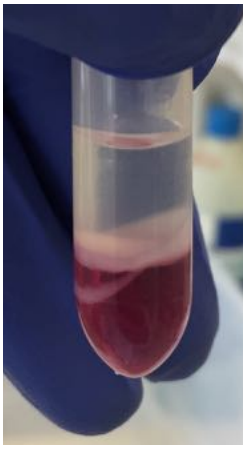

***Figure 2.3: Representative picture of phase separation***
*After homogenizing the distinct brain regions in InnuSolv Reagent, incubation with chloroform and centrifugation three phases can be differentiated in the Eppendorf Tube®. The upper, colorless phase contains mRNA, the white intermediate phase DNA and the red lower organic phase contains protein.*

### 2.2.4 RNA isolation

The upper transparent RNA containing phase was transferred to a new 1.5 ml Eppendorf Tube and immediately put on ice. The intermediate phase was discarded and organic phase stored at 4°C up to one week until further processing.
To precipitate RNA 500 µl isopropanol and 1 µl glycogen (Thermo Scientific, Austria) were added. Glycogen is an inert, in isopropanol insoluble polysaccharide, which helps forming a visible pellet during centrifugation. Tubes were inverted for five times to mix the components

and incubated at room temperature for 10 min before centrifugation at 12000xg and 4°C for 8 min.

Isopropanol was discarded carefully. When no pellet could be seen, special attention was paid to ensure not touching the area with the pipet tip, where the RNA should have deposited during centrifugation. RNA was washed twice, each time with 1 ml of 75% ethanol followed by centrifugation at 7500xg and 4°C for 5 min. After the second washing step, ethanol was completely removed working under a lamina, which was UV sterilized and cleaned with RNAse decontamination solution (Molecular BioProducts, US). Afterwards tubes were left open for a maximum of 10 min so that the remaining traces of ethanol could evaporate. When the pellet was completely dry it became transparent.

Finally, the RNA pellet was dissolved in 30 µl of DEPC treated nuclease free water (VWR, Austria). After 10 min incubation at 60°C and 350 rpm in a thermomixer (Eppendorf, Germany) tubes were immediately put back on ice. RNA content was measured with NanoDrop (Thermo Scientific, Austria) and the mRNA stored at -80°C.

### 2.2.5 RNA integrity

mRNA isolated from different brain parts of pre-test mice (see chapter 2.2.1) was tested on TapeStation4200 (Agilent, Austria) to check RNA integrity and quality prior to the main experiments. Preparation was done according to the manufacturer's protocol using 200 ng RNA per sample.

In brief, 1 µl of a RNA ladder or 1 µl of the RNA sample containing 200 ng RNA were diluted with 5 µl of RNA sample buffer in a tube strip, vortexed and spun down. Diluted RNA-ladder and samples were denatured for 3 min at 72°C and afterwards placed on ice for 2 min to cool down. Then samples were loaded into the TapeStation instrument, which performs gel electrophoresis of the RNA and analyses its quality and quantity. Therefore the line intensity of 18S and 28S band, representing ribosomal RNA, is determined in the corresponding electropherogram and the ratio between these two is calculated by the TapeStation Software.

### 2.2.6 DNA digestion and reverse transcription to cDNA

DNase digestion and reverse transcription into cDNA were performed under UV disinfected and with RNase decontamination solution cleaned lamina, always keeping the samples on ice to avoid contamination with gDNA or degradation of RNA. Enzymes were kept in -20°C - cooling racks.

For each sample, the required volume of dissolved RNA corresponding to a total amount of 2000 ng of mRNA per sample was calculated based on the NanoDrop measurements, pipetted into PCR tubes, and made up to 7 µl with nf-H2O.
In cases, where the volume of dissolved RNA exceeded the maximum of 7 µl, because the RNA amount was very small, only these possible 7 µl were used for DNAse digestion and reverse transcription into cDNA and the ratios were considered later at preparing mastermixes for qPCR. 2 µl (2 u) of DNase I and 1 µl of 10x reaction buffer with $MgCl_2$ from DNase I, RNase-free kit (Thermo Scientific, Austria) were added to 7 µl of RNA for DNA digestion before 30 min incubation at 37°C.
mRNA stocks were stored at - 80°C.
To deactivate DNase I enzyme 1 µl of 50 µM EDTA were added to each sample. The samples were incubated at 65°C for 10 min to finally denature the enzyme.

Reverse transcription was performed using High-Capacity cDNA Reverse Transcription Kit (Applied Biosystems, Austria). 9 µl of the mastermix were added to the samples directly after the DNAse inactivation step. This mastermix consisted of the following components per sample: 2 µl of reverse transcriptase buffer, 0.8 µl of 100 mM dNTPs-mix, 2 µl of 10x reverse transcriptase random primer (Applied Biosystems, Germany), 0.25 µl of RiboLock RNase inhibitor (Thermo Scientific, Austria), 1 µl of the multiscript reverse transcriptase (50 U/µl) and 2.95 µl of nf-$H_2O$.
Then cDNA synthesis was performed with thermal cycler PCR System 9700 GeneAmp (Thermo Scientific, Austria) using the following temperature protocol.

***Table 2.8:*** *Temperature protocol for reverse transcription of mRNA to cDNA*

| Step | 1 | 2 | 3 | 4 |
|---|---|---|---|---|
| Temperature, [°C] | 25 | 37 | 85 | 4 |
| Time, [min] | 10 | 120 | 5 | ∞ |

Afterwards samples were diluted with 20 µl nf-$H_2O$ each, resulting in 40 µl cDNA samples, which were stored at -20°C.

### 2.2.7 Primer design and validation

FASTA sequences of the protein coding genes of mus musculus (taxid: 10090) were looked up at NCBI nucleotides. Primers of these sequences were designed using NCBI primer-blast (Ye at al. 2012). If there were different transcript variants, primers were designed to cover as many of them as possible.

PCR product size was reduced to a maximum of 200 bp to ensure high primer efficiency. Primer melting temperatures ($T_m$) were changed to min = 60°C, Opt = 63°C, max = 66°C. The temperature increase by 3°C was necessary to minimize unspecific primer binding. In addition, primers were designed to span exon-exon junctions and to exclude possible influences of gDNA residues. The remaining parameters were kept at standard settings. Primers were picked to have a low Self and Self 3' complementarity and at best no products on other unintended targets than transcript variants of the same gene.

Primers for the following murine genes were included in this study: RPL4 - ribosomal protein L4, UCP4 - uncoupling protein 4, GLUT3 - glucose transporter 3, MCT2 - monocarboxylate transporter 2, Gck - glucokinase, CACT - carnitin-acylcarnitin-transporter, CPT1c - carnitine palmitoyltransferase 1c, CPT2 - carnitine palmitoyltransferase 2, PLIN3 - perilipin 3, SOD1 - superoxide dismutase 1, PGC1a - peroxisome proliferator-activated receptor gamma coactivator 1-alpha (Tab. 2.4).

Primers were solubilized according to manufacturer's instructions with nf-$H_2O$ after their arrival. These primer stocks (c=100 µM) were diluted by adding 10 µl forward and 10 µl reverse primer of the same gene into 980 µl of nf-$H_2O$ to get a final concentration of 1 pmol/µl. These aliquots were used for the following experiments.

To check primer efficiency, a serial dilution of pooled cDNA of two different pre-test restbrain samples was used. 11 PCR master mixes were made, each containing 5 µl Luna (New England Biolabs, Germany), 1.5 µl nf-$H_2O$ and 0.5 µl cDNA in different dilutions ranging from 1:1 to 1:1024 for one reaction. The different concentrations were prepared as serial dilution, every time mixing 1 ml nf-$H_2O$ with 1 ml of the previous concentration, starting with the stock solution. A 384 well plate was used for efficiency check. Pipetting of this plate was performed by the pipetting robot epMotion 5075 (Eppendorf, Austria) starting with 3 µl primer solution in each well followed by 7 µl of master mix containing Luna and cDNA. No template controls (NTC) were included in the experiment, where cDNA was replaced with nf-$H_2O$. During the efficiency test also reverse transcription controls (Rt-) were tested once, to validate the

specificity of the PCR process, or more precisely, whether the primers bind cDNA only and not gDNA. This control was not performed in main runs.
The RT-qPCR was run on qTower3 84 (Analytik Jena, Germany), with an annealing temperature set to 62°C, after preheating the lid to 100°C with the following cycling protocol. Optimal annealing temperature being 62°C was already known from a previous study (Felix Locker, unpublished results).

***Table 2.9:*** *RT-qPCR temperature protocol*

| Step | | Temperature (°C) | Time (m:s) | goto | loops | scan |
|---|---|---|---|---|---|---|
| 1 | Initial Denaturation | 95 | 01:00 | | | |
| 2 | Denaturation | 95 | 00:15 | | | |
| 3 | Annealing | 62 | 00:30 | | | |
| 4 | Extension | 72 | 00:30 | 2 | 44 | yes |
| 5 | Melting curve | | 00:15 | | | yes |

Gel electrophoresis of the corresponding amplicons to each primer was performed. A 3% Agarose gel was prepared using TBE buffer (Tab. 2.10) and 10 µl SYBR gel stain (Thermo scientific, Austria) for 100 ml gel. 10 µl of RT-qPCR products were diluted with 2.5 µl Bromphenolblue (Sigma-Aldrich, Austria). In each pocket of the gel 6 µl of the diluted products were loaded. Hyperladder (Bioline, UK) and 100 bp ladder (NEB, Germany) was used as a marker. After separation of the bands at 120 V for 10 min followed by 55 min at 200 V, they were visualized using UV-illumination at 256 nm with gel documentation and fluorescence imaging system Quantum (Vilber, Germany)

***Table 2.10:***

| 10x TBE buffer (1000 ml) | |
|---|---|
| Tris | 108 g |
| Boric acid | 55 g |
| 0.5M EDTA pH 8 | 40 ml |
| →needs to be diluted 1:10 before usage | |

### 2.2.8 RT qPCR

Based on efficiency tests, we estimated the optimal dilution for cDNA with the premise that the $C_t$ for all used primers fell into their linear range. For cDNA samples, where 2000 ng could be used for cDNA synthesis, we used a dilution of 1:8. In the case that less RNA could be extracted and used for cDNA synthesis, dilution was lowered accordingly, so that amplification started with approximately the same amount of cDNA in each well. 384 well plates were used to test each cDNA sample with every primer in triplicates. Each well of the plate contained all together 7.5 µl reaction volume, including 3.75 µl Luna, 0.375 µl cDNA, 2.25 µl primer solution and filled up with nf-H20 to the end volume. Volume was decreased in contrast to the procedure as described for primer efficiency test. No template control (NTC) was tested in duplicates. Pipetting and RT-qPCR temperature setup were performed as described before.

### 2.2.9 Protein isolation with InnuSolv Reagent

Protein was precipitated out of the organic phase using 750 µl isopropanol for cerebellum and restbrain and 1.5 ml isopropanol for hippocampus and hypothalamus for 10 min at room temperaure (RT). Higher amounts of isopropanol resulted in a better precipitation of proteins but also of other anorganic components.

After incubation samples were centrifuged 10 min at 12000xg and 4°C. Supernatant was discarded and the pellet was washed three times with 1 ml 0.3 M guanidinhydrochlorid (GdmCl) in 95% ethanol, every time with an incubation of 20 min at RT before centrifugation and changing wash solution. After the third time the washing solution was removed completely and the pellet was vortexed in >99,9% ethanol followed by another 20 min incubation at RT to dissolve the rest of GdmCl out of the pellet. The pellets were stored in >99,9% ethanol for a maximum of one year until solubilization. Proteins were solubilized with 1% SDS solution after drying them fully in a thermomixer (50°C, 400 rpm) with opened lids. The amount of 1% SDS solution depended on the size of the pellet and varied between 60 µl for hypothalamus up to 400 µl for the restbrain. After fragmenting the pellet with a needle, it was incubated for 2 min at 50°C followed by 8 min at 60°C. Then the protein solution was sonicated three times for 3 s on ice, incubated for half an hour on ice and centrifuged before collecting the supernatant for storage at -20°C to -80°C.

### 2.2.10 Protein isolation with RIPA buffer

To rule out isolation-dependent effects (e.g. resolubilization of the pellets, protein degradation) on protein expression levels we included an additional protein isolation method in this study. Protein was isolated using a lysis buffer consisting of RIPA buffer (Tab. 2.11)

and protease inhibitor cocktail (Sigma-Aldrich, Austria). For each sample a volume of approximately ten times its weight was used.

| ***Table 2.11:*** | |
|---|---|
| RIPA buffer (250ml) | |
| Tris | 1.51 g |
| NaCl | 2.19 g |
| Desoxycholic acid sodium salt | 2.5 g |
| Triton X-100 | 2.5 ml |
| EDTA | 0.093 g |
| SDS | 0.25 g |
| + HCl | pH 7.4 |

After homogenization with a MixerMill 200 (Retsch, Germany) using wolframcarbid beads, the samples were sonicated using ultrasound device (Branson Ultrasonics Corporation, US) one time for 3 s and incubated for half an hour on ice. Then they were centrifuged with 1000xg at 4°C, supernatant was centrifuged again with 2500xg at 4°C for ten minutes. Then this time supernatant was collected and stored at -20°C.

### 2.2.11 Protein determination

Regardless of the protein isolation method, protein concentration was measured using Pierce™ BCA Protein Assay Kit (Thermo Scientific, US) for a 96 well microplate. Aliquots of the original proteins were diluted 1:25 with distilled water before measurement. 10 BSA standards ranging from 50 µg/ml to 900 µg/ml were prepared for the standard curve.
In each well either 25 µl of water (blank), standard or diluted protein and 200 µl of working reagent were pipetted and then immediately incubated at 37°C for half an hour. Then, absorbance was measured at 562 nm with EnSpire 2300 Multilabel reader (PerkinElmer, Germany) and protein concentrations were calculated based on the standard curve with Excel.

### 2.2.12 Western Blot procedure

20 µg of protein of either hypothalamus, or hippocampus, or cerebellum or restbrain of each diet experiment diluted with loading dye were loaded on 0.75 mm thick SDS gels, consisting

of 3.75% stacking and 12% separating gel (Tab. 2.12). Mini-PROTEAN® Tetra handcast system was used to cast and run the polyacrylamide gels.

***Table 2.12:*** *Composition of polyacrylamide gels*

| 12% separating gel 1x | | 3,75% separating gel 1x | |
|---|---|---|---|
| Tris 2 | 1 ml | Tris 1 | 0.5 ml |
| Acrylamid | 1.6 ml | Acrylamid | 0.25 ml |
| Bisacrylamid | 0.64 ml | Bisacrylamid | 0.10 ml |
| $ddH_20$ | 0.76 ml | $ddH_20$ | 1.15 ml |
| TEMED | 5 µl | TEMED | 2.6 µl |
| APS | 40 µl | APS | 20 µl |

***Table 2.13:*** *Tris buffer solutions*

| TRIS1 (1000ml) | | TRIS2 (1000ml) | |
|---|---|---|---|
| Tris | 60.6 g | Tris | 181.6 g |
| SDS | 4 g | SDS | 4 g |

For each brain region a set of eight gels was loaded: two membranes representing the fasting conditions with SD, IF and CR and two membranes for the KDs with SD, LCT and LCT-MCT. Four other membranes were duplicates of the previously described ones. For each diet experiment samples of eight animals were included. On the set of gels corresponding to the KDs consistent to the purpose to have a better statistics, four samples of the first feeding trial from 2019 isolated with InnuSolv and four samples of the second feeding trial 2021 isolated with RIPA buffer were loaded on the gels. As a positive control 1 µg inclusion bodies containing recombinant UCP4 as well as 10 µg brain standard were pipetted on the gels. 20 µg of spleen standard were used as a negative control, because UCP4 is not abundant in spleen (Smorodchenko et al. 2009). Brain and spleen standard contain pooled tissue from more than one mouse and were previously isolated in our laboratory using RIPA buffer. For the investigation of UCP4 distribution and amount of neurons, astrocytes and microglia in the distinct brain regions, samples of the five mice fed the SD in 2021, which were isolated with RIPA buffer, were included for each brain region.

Furthermore, lysates of sorted cells, either neurons, astrocytes or microglia (n=2 for each cell type), obtained by a cooperation partner (M. Maes, IST, Klosterneuburg, Austria) and previous experiments of our lab (A. Rupprecht), isolated with RIPA buffer, were analyzed by Western Blot to compare UCP4 in the individual cell populations. The protein samples were diluted in loading dye (Tab. 2.14) before loading them on the gels. Precision Plus Protein Dual Color Standard (BioRad, US) was used for molecular weight estimation. Each time four gels were run together in an electrophoresis tank (Biorad Mini Protean® Tetra cell) in running buffer (Tab. 2.15) starting with 30 min at 50 V and afterwards at 120 V as long as the 15 kDa band of the marker reached the end of the gel.

| ***Table 2.14:*** | |
|---|---|
| 4x loading dye (100ml) | |
| Tris | 1.21 g |
| SDS | 4 g |
| Glycerin | 10 ml |
| ß-mercaptoethanol | 4 ml |
| Bromphenolblue | 1 pinch |
| dd$H_2O$ | 80 ml |

| ***Table 2.15:*** | |
|---|---|
| 10x Electrophoresis buffer WB (2000 ml) | |
| Tris | 60.58 g |
| Glycine | 288.24 g |
| SDS | 20 g |
| →needs to be diluted 1:10 before usage | |

Afterwards electrophoresis gels were transferred to nitrocellulose membranes (Amersham Protran 0.45 µm NC, GE Healthcare, US) for 1 h at 14 V using a semi-dry blotter (Peqlab, Germany) and methanol containing Blot buffer (Tab. 2.16).

| ***Table 2.16*** | |
|---|---|
| Blot buffer for Nitrocellulose, RT (2000ml) | |
| Tris | 6.06 g |
| Glycine | 28.84 g |
| Methanol | 400 ml |

Then the membranes were stained with Ponceau S solution to verify successful blotting and visualize total protein. After blocking the membranes for 1 h in 2% BSA blocking solution at RT, they were incubated with primary antibodies overnight at 4°C in plastic cuvettes on a

shaker. Primary antibodies were diluted as indicated in the table 2.5. The anti-UCP4 antibody (see chapter 2.2.13) was diluted 1:5000. All primary and secondary antibodies ,like UCP4, mitochondrial markers (voltage dependent anion channel (VDAC), Complex II (SDHA), Oxoglutarate Dehydrogenase (OGDH)), ß actin and Neuronal Nuclei (NeuN), were diluted with 2% BSA block solution, except Glial fibrillary acidic protein (GFAP) and Ionized calcium-binding adapter molecule 1 (IBA1) antibodies, which were diluted in 5% nonfat dry milk according to manufacturer's instructions to minimize a background.

***Table 2.17***

| Ponceaustaining for nitrocellulose, RT (1000ml) | |
|---|---|
| Ponceau S | 0.2 g |
| Trichloroacetic acid | 3 g |

***Table 2.18***

| 2% BSA Blocksolution, 4°C (1000ml) | |
|---|---|
| 10 x TBS | 100 ml |
| BSA | 20 g |
| Tween 20 | 500 µl |
| Thimerosal (0,02%) | 2 ml |

At the next day membranes were washed three times in 1x TBS-T (Tab. 2.20) and were incubated for 1 h at RT with the secondary antibody coupled to HRP, followed by another three washing steps. For visualization of the antibody binding membranes were incubated with Clarity™ Western ECL Substrate for 5 min. For detection of the bands Chemidoc IT 600 Imaging System (UVP, UK) was used.

For normalization of the proteins of interest, VDAC, SDHA and ß-actin were detected on the same membranes subsequently. In between different primary antibodies membranes were stripped with strip solution (Tab. 2.21) for 5-15 min depending on the strength of chemolumineszence of the previous antibody. To confirm the purity of the samples for the analysis of UCP4 in different cell populations (see chapter 3.5), GFAP and IBA were also detected following UCP4 on the corresponding membranes.

| *Table 2.19* | |
|---|---|
| 10 x TBS buffer, 4 °C (1000ml) | |
| Tris | 60.58 g |
| NaCl | 87.66 g |
| pH = 7.4 (+ 37% HCL) | |

| *Table 2.20* | |
|---|---|
| 1 x TBS-T buffer, 4 °C (1000ml) | |
| 10x TBS | 100ml |
| ddH20 | 900ml |
| Tween20 | 500µl |

| *Table 2.21* | |
|---|---|
| Strip solution, 4 °C (1000ml) | |
| Natriumcitrate | 29.4 g |
| pH = 2.2 (+ 37% HCL) | |

### 2.2.12 Western Blot analysis

For the semi-quantitative analysis it was important to check, whether the line intensity quantified in the Western Blot was linearly dependent on the amount of protein. Therefore, we first analyzed six different dilutions of the brain lysates starting with 22.5 µg protein per lane and decreasing with dilution factor 0.67. For further experiments we used an amount of total protein, that corresponded to values located in the linear range (Pillai-Kastoori, 2020).
Semi-quantitative analysis of the Western Blots was done using Software VisionWorks 8.20 (Analytik Jena, Germany). Background correction was performed using „Joined valleys“, the sensitivity value was set to ten.
Line intensity of the target proteins ($i_{TP}$) representing protein expression was related to the line intensity of the mitochondrial markers (VDAC, SDHA, OGDH) and ß-actin ($i_{HK}$) as a cellular housekeeping protein ($i_x = i_{TP}/i_{HK}$ = relative protein amount). These ratios were normalized either to the mean values determined for the SD or to the brain standards loaded on the corresponding membranes. Since for the investigation of protein expression upon the different diets every sample was loaded in duplicates on different membranes, the average of both normalized values was calculated and used for statistical analysis.

### 2.2.13 UCP4 antibody production and validation

For the planned experiments a new charge of the specific anti-UCP4 antibody was produced and validated as previously described in Smorodchenko et al. (2009). Pre-immunsera of four different rabbits obtained from PINEDA Antibody Service GmbH (Berlin, Germany) were

tested in a dilution of 1:5000 on membranes, on which total proteins of UCP4-positive samples like brain and neurons and the UCP4 negative tissues spleen, liver and heart were blotted. Membranes were incubated overnight in the sera and washed three times in TBS-T solution (Tab. 2.20). HRP-linked secondary rabbit antibody was added for 1 h at RT and washed again three times before visualizing antibody binding with Clarity™ Western ECL Substrate. The pre-immune sera of the two rabbits with the lowest background at the weight corresponding to UCP4 molecular weight (36kD) were selected for immunization. Peptide synthesis and immunization of rabbits with UCP4-1 N terminal peptide sequence KLLPLTQRWPRTSK (Smorodchenko et al. 2009) was performed by Pineda Antikörper-Service (Berlin, Germany).

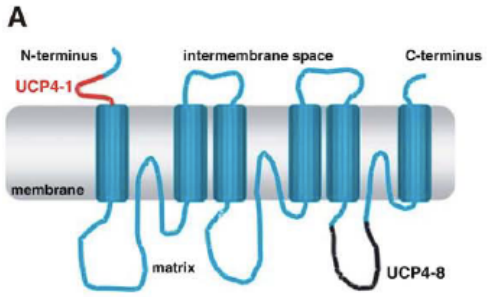


***Figure 2.4: UCP4 putative structure***
*The peptide, which was used for antibody production is marked red. Taken from Smorodchenko et al. 2009*

Affinity-purified antibodies sent to us at day 60, 90, 120 and 150 post immunization were tested like described before for pre-immune sera, always using a dilution of 1:5000 for primary and secondary antibodies to monitor efficiency of antibody production. Final exsanguination was accomplished on day 165 after immunization. Antibodies purified according to the manufacturer's quality specifications and sent to us were tested (Suppl. Fig. 5), aliquoted and stored at -80 °C until further usage.

### 2.2.14 Statistical analysis

Data of UCP4 gene and protein expression were analyzed using GraphPad Prism software.
PCRs and statistical analysis for gene expression were performed with three technical replicates each for eight biological replicates.
Gene expression differences were first calculated with $\Delta c_t$ method and then, because more than two groups were to be compared, analyzed using a one-way ANOVA with Kruskal-Wallis test for non-parametric Data and Dunn’s multiple comparisons test.

Data from KDs (LCT, LCT/MCT) and fasting experiments (IF, CR) were compared to standard diet (SD) respectively.

For generation of the heat map with GraphPad Prism, the mean values of each of the eight biological replicates were divided by the mean value of the SD, resulting in the SD taking the value of one (white). Calculations were done with Excel. The normalized means of the other diets were color-coded as higher (>1, red) or lower (<1, blue) than SD. No significances can be concluded from this presentation.

To create the correlation analysis, gene expression data of the hippocampus were plotted in an xy-diagram with a logarithmic scale. Each value in the graph corresponds to the sample of one mouse, with the abscissa indicating the expression of one gene and the ordinate indicating the expression of the gene to be compared. Based on the individual values, the regression line was determined and is shown in the graph. Pearson correlation coefficient (r) was calculated.

Protein expression was analyzed with ordinary one-way ANOVA using Dunnetts multiple comparisons test, as we assume normally distributed data in this case.

Western blot data were derived from five biological replicates when comparing brain regions, and from eight biological replicates with two technical replicates each when comparing diets.

Outliers were calculated using GraphPad online calculator which performs Grubbs' test. The significance level (alpha) was defined to be 5%.

Data are presented as mean values +/- Standard Error of Mean (SEM). Individual data points are presented. Significant differences are indicated with: * $P \leq 0.05$, ** $P \leq 0.01$, *** $P \leq 0.001$.

# 3. Results

## 3.1 RNA integrity

To obtain reproducible qPCR-results which reflect the specific gene expression of one individual, it is very important to use intact RNA for cDNA synthesis. Since RNase enzymes are pervasive, RNA gets rapidly digested when the extraction protocol is not optimized. RNA integrity is mainly defined by the ratio of ribosomal bands 28S:18S. These bands can be displayed using gel-electrophoresis. Agilent TapeStation4200, which was used for this experiment, automatically calculated RNA integrity number (RIN) after electrophoresis, representing the degradation of RNA on a ten-point scale. Thereby RIN=1 stands for totally degraded and RIN=10 for intact RNA.

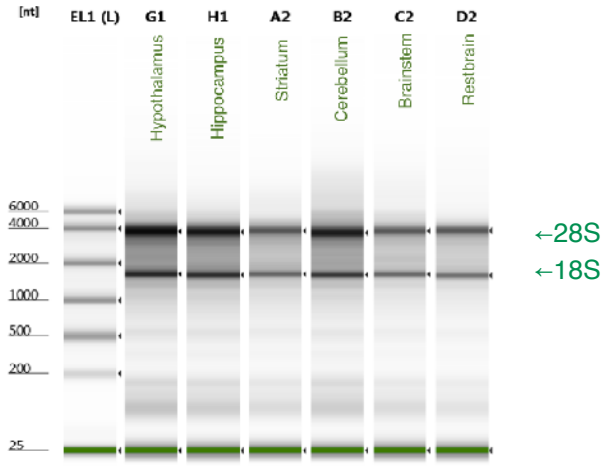


***Figure 3.1: Representative RNA gel electrophoresis image generated by TapeStation4200***
*To preclude disruptive effects of RNA degradation on gene expression analysis, RNA integrity was tested. 200 ng RNA extracted of hypothalamus, hippocampus, striatum, cerebellum, brainstem and restbrain, were diluted in ScreenTape sample buffer and loaded on a RNA ScreenTape on each lane respectively. The gel image shows two well-defined bands (28S, 18S) and almost no RNA degradation. Table 3.1 shows the RNA integrity numbers of this experiment.*

***Table 3.1:*** *RNA integrity numbers*

| Lane | Tissue | RIN |
|---|---|---|
| EL1 | Ladder | - |
| G1 | Hypothalamus | 8.6 |
| H1 | Hippocampus | 8.7 |
| A2 | Striatum | 8.3 |
| B2 | Cerebellum | 8.7 |
| C2 | Brainstem | 8.8 |
| D2 | Restbrain | 8.9 |

Since all of our RIN numbers are higher than eight, as listed for one representative experiment in the table 3.1, and two well delimitable bands and low degradation could be

visualized on the gel image (see Figure 3.1) RNA quality can be considered high. The suitability of the extraction method for further gene expression analysis with RT-qPCR can be confirmed.

## 3.2 Primer validation

Based on the gene expression data of a serial dilution of pooled restbrain cDNA samples from pre-test mice (see chapter 2.2.7) ranging from 1:1 to 1:1024 in 11 steps, a standard curve was generated plotting $C_t$ on the y-axis vs the decadic logarithm of the dilution factor on the x-axis. The slope of the standard curve, primer efficiency and coefficient of determination were calculated for each primer (Bustin and Huggett, 2017). Primers were accepted when their efficiency ranged between 89% and 105%. The coefficient of determination ($R^2$) of the fitted regression line needed to be at least 0.995. A broad linear range could be shown for all used primers except Gck and MCT2. Exact values are shown in the table. 2.4.

Unfortunately, glucokinase primer could not fulfill the criteria. It was indeed used as well for gene expression studies because of its role as rate limiting enzyme of glycolysis (Liu, 2006). It is known that Gck is especially expressed in hypothalamus. As we did not perform the initial efficiency test with hypothalamus, a precise answer about the mGck primer is missing and should be performed in future studies.

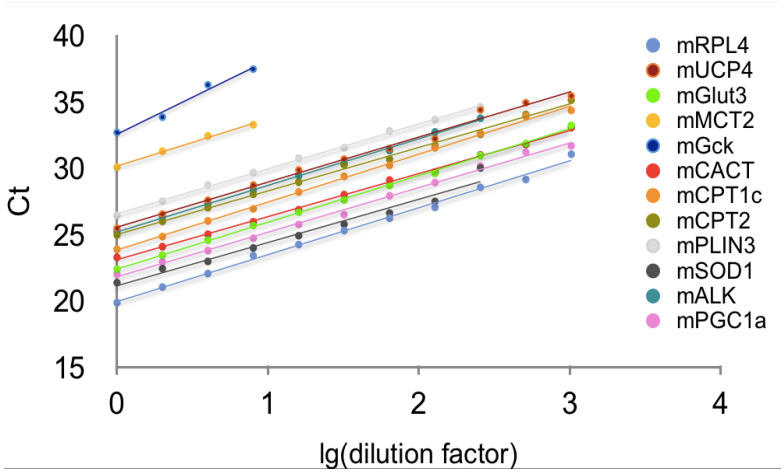


***Figure 3.2: Standard curves of the primer efficiency tests.***
*To accurately quantify the number of copies of mRNA in different samples, the primer should have a wide linear dynamic range. The linear ranges of each primer which is included in further experiments are plotted in the diagram as Ct (cycle threshold) as a function of the dilution level (lg(dilution factor)) of the cDNA. For each primer, the expression at each dilution is plotted (n=3) Furthermore, the regression line is shown. The slope is given in table 2.4.*
*RPL4 - ribosomal protein L4, UCP4 - uncoupling protein 4, GLUT3 - glucose transporter 3, MCT2 - monocarboxylate transporter 2, Gck - glucokinase, CACT - carnitin-acylcarnitin-transporter, CPT1c - carnitine palmitoyltransferase 1c, CPT2 - carnitine palmitoyltransferase 2, PLIN3 - perilipin 3, SOD1 - superoxide dismutase 1, PGC1a - peroxisome proliferator-activated receptor gamma coactivator 1-alpha*

To check if the true size of the PCR products matches the in silico predicted size of the amplicons to verify correct primer binding, the qPCR products of all primers included in this study were loaded onto an agarose gel to perform electrophoresis and afterwards visualized with UV light.

Gel electrophoresis of the amplicons proved that primer binding results in the amplification of genes the primers were designed for and no unintended targets, since all products had the expected sizes (Fig. 3.3)

| lane | 1 | 2 | 3 | 4 | 5 | 6 | 7 | 8 | 9 | 10 | 11 | 12 | 13 | 14 | 15 |
|---|---|---|---|---|---|---|---|---|---|---|---|---|---|---|---|
| Primer | 100bp ladder | **mRPL4** | **mUCP4** | **mGlut3** | **mMCT2** | **mGck** | **mCACT** | 100bp ladder | **mCPT1c** | **mCPT2** | **mPLIN3** | **mSOD1** | **mALK** | **mPGC1a** | 100bp ladder |
| predicted size | | 124bp | 101bp | 180bp | 72bp | 117bp | 109bp | | 181bp | 98bp | 83bp | 71bp | 157bp | 83bp | |

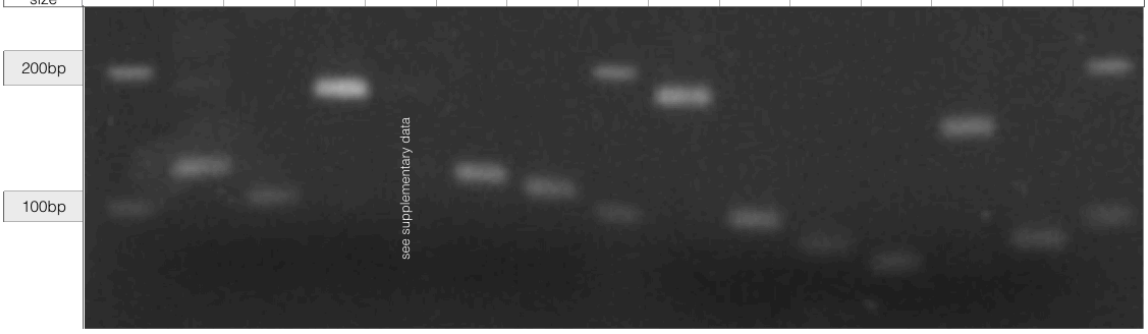


***Figure 3.3: Representative picture of PCR products after gel electrophoresis***
*Predicted sizes of the amplicons for each primer are given in the table above the gel picture. The actual size of the amplicons (in basepairs, bp) can be estimated by comparing the height of the bands in the gel with the markers loaded in lane 1, 8 and 15.*
*RPL4 - ribosomal protein L4, UCP4 - uncoupling protein 4, GLUT3 - glucose transporter 3, MCT2 - monocarboxylate transporter 2, Gck - glucokinase, CACT - carnitin-acylcarnitin-transporter, CPT1c - carnitine palmitoyltransferase 1c, CPT2 - carnitine palmitoyltransferase 2, PLIN3 - perilipin 3, SOD1 - superoxide dismutase 1, ALK- anaplastic lymphoma kinase , PGC1a - peroxisome proliferator-activated receptor gamma coactivator 1-alpha*
*For the amplicon of mMCT2 primer see supplementary data.*

## 3.3 Expression of UCP4 and other genes involved in the neuronal metabolism

Amount of UCP4, genes involved in fatty acid metabolism or glucose metabolism or SOD1, as a marker for oxidative stress were analyzed in four brain regions (hypothalamus, hippocampus, cerebellum and restbrain). These tissues originated from 40 mice out of five different feeding groups.

Delta Ct (ΔCt) method was used to normalize the genes of interest to RPL4 as a housekeeping gene (HKG), meaning that the Ct value of the HKG is subtracted from the Ct values of the gene of interest. Afterwards relative values are achieved by using ΔCt as a negative exponent to 2 (=$2^{-\Delta Ct}$)

$2^{-\Delta Ct}$ values were calculated and plotted in graphs. In order to create a heatmap of gene expression, the fold change towards SD was calculated for every animal and the mean of every feeding group was plotted.

### 3.3.1 Impact of diets on housekeeping gene expression

Previous results of our lab and others (de Jonge et al. 2007) indicated RPL4 to be a very stable housekeeping gene (HKG). However, slight but significant changes in gene expression could be observed within the different feeding groups depending on the brain regions, although the same amount of RNA was used during the whole experiment.

RPL4 gene expression was downregulated in restbrain and upregulated in cerebellum upon LCT/MCT feeding. We could also show upregulation in the CR group in hippocampus. mRPL4 transcripts were upregulated in all feeding groups except LCT, compared to SD in hypothalamus (Fig. 3.4)

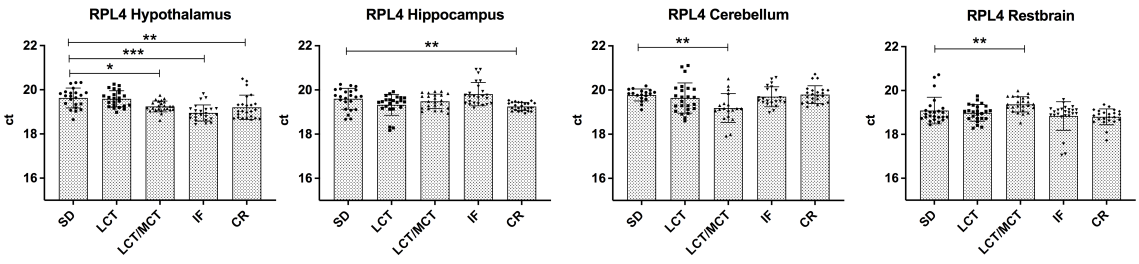


***Figure 3.4: Expression of the housekeeping gene mRPL4 upon different diets in different brain regions***

*To analyze possible effects of the diets on the HKG mRPL4, triplicates of each brain sample (n=8) were analyzed with qPCR and absolute mRNA levels were plotted. The bars represent mean ± SEM. LCT, LCT/MCT, IF and CR were compared with SD using one-way ANOVA. Significant differences (P-values) are marked with *P ≤ 0.05, ** P ≤ 0.01 and ***P ≤ 0.001.*
*SD-standard diet, LCT-long chain triglycerides, LCT/MCT-long and medium chain triglycerides, CR-caloric restriction, IF-intermitted fasting, RPL4- ribosomal protein L4, ct-cycle treshold*

Hence, only normalization of the gene expression to RPL4 in restbrain upon LCT/MCT diet might influence the relative values.

Since other changes do not lead to significant changes in the normalized data, they can be neglected in this case. However, for further experiments, at least two more HKGs should be included to obtain more valid values.

### 3.3.2 Effects of different diets on the expression of metabolically active genes

Our data showed that change in nutrient availability affects the gene expression in various brain regions differently.

The hippocampus and cerebellum as they were reported to express high levels of UCP4 (Ramsden et al. 2012) were analyzed now upon different diets. The same high expression of UCP4 mRNA under standard conditions applies to restbrain, where the cortex accounts for a major proportion (Smorodchenko et al. 2009).

Hypothalamus was analyzed due to its essentially integrative role by processing sensory input to make important decisions about basic life functions (Saper and Lowel 2014). For example metabolic sensing neurons, prior in the ventromedial hypothalamus, can be altered by a broad spectrum of metabolites (Le Foll and Levin 2016) and are highly responsive to any changes in metabolism.

We investigated the expression of GLUT3 and Gck for the glycolytic pathway and PLIN3, CACT, CPT1c and CPT2 for usage of FA. We intended to observe an increase of oxidative stress by increase in expression of cytoplasmic SOD1. To examine the state of ketogenesis we used primers for mMCT2, the neuronal transporter for ketone bodies and mPGC1a, the master regulator of mitochondrial biogenesis, which is activated at low carbohydrate levels (Wallace et al. 2010), as is the case in our ketogenic diet.

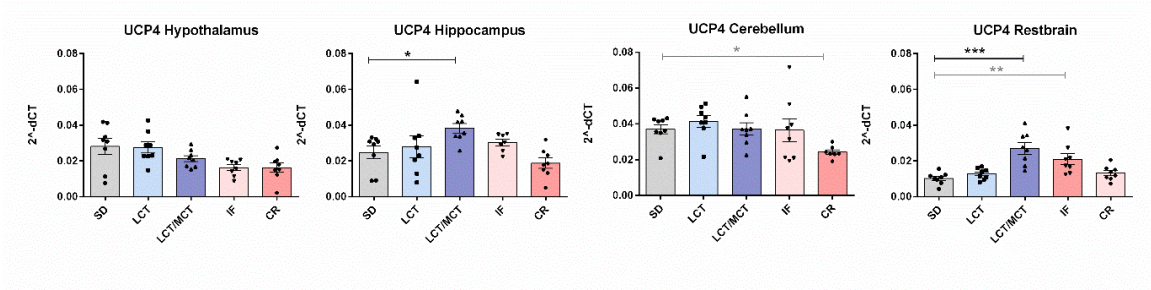


***Figure 3.5 UCP4 mRNA expression in four brain regions***

*Samples were analyzed in triplicates with n=8 biological replicates and distinct data points of relative gene expression ($2^{-\Delta Ct}$) normalized to RPL4 for each animal were plotted, the columns depict the values as mean ± SEM. LCT, LCT/MCT, IF and CR were tested against SD respectively using one-way ANOVA, significant differences (P-values) are marked with *P ≤ 0.05, ** P ≤ 0.01 and ***P ≤ 0.001. SD-standard diet, LCT-long chain triglycerides, LCT/MCT-long and medium chain triglycerides, CR-caloric restriction, IF-intermitted fasting.*

Significant upregulation of UCP4 gene expression can be observed upon LCT/MCT in hippocampus and downregulation upon CR in the cerebellum. Since we aimed to show connections between UCP4 gene expression and other metabolically active proteins we plotted the complete data set into an heatmap after dividing the mean $2^{-\Delta Ct}$ values of LCT, LCT/MCT, IF and CR by the $2^{-\Delta Ct}$ values of the SD for each primer respectively, thereby setting SD to one (see chapter 2.2.14). The significance must be taken in each case from the individual representations of the genes (Fig. 3.7, 3.8, 3.9)

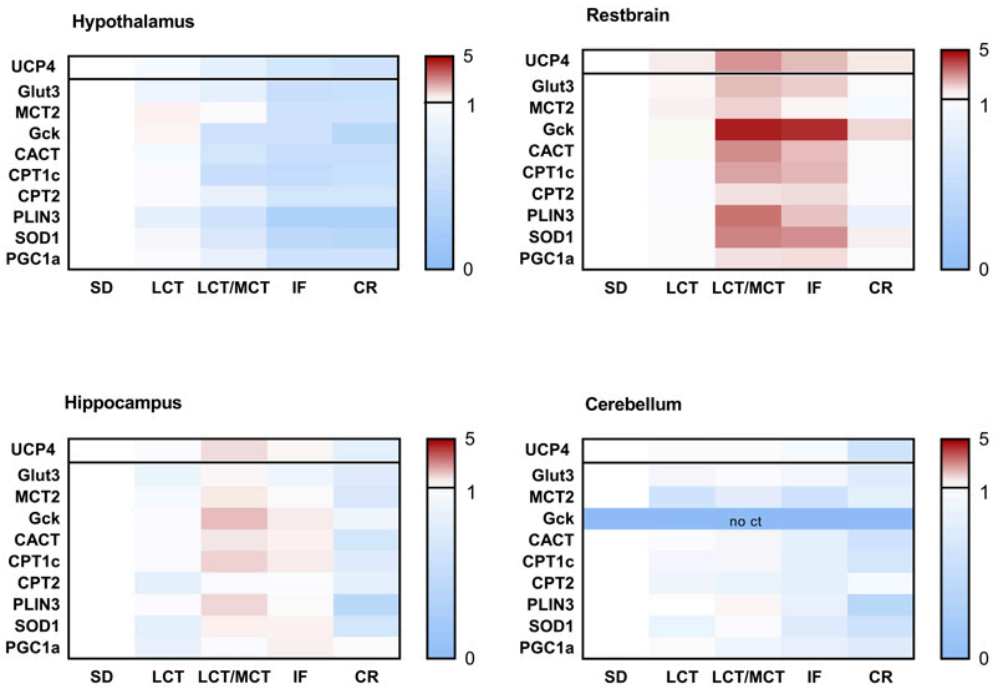


***Figure 3.6: Gene expression heatmap***

*Heatmap displaying relative expression of mUCP4 and genes associated with different metabolic pathways in the hypothalamus ,hippocampus, cerebellum and restbrain. Relative mRNA levels normalized towards RPL4 are shown for each feeding group and region.Therefore SD was set to 1 and the mean of the values for each primer is plotted respectively. Color indicates the magnitude of change in gene expression toward SD in 0-5 fold.*

*SD-standard diet, LCT-long chain triglycerides, LCT/MCT-long and medium chain triglycerides, CR-caloric restriction, IF-intermitted fasting*

*UCP4-uncoupling protein 4, GLUT3-glucose transporter 3, MCT2-monocarboxylate transporter 2, Gck-glucokinase, CACT-carnitin-acylcarnitin-transporter, CPT1c-carnitine palmitoyltransferase 1c, CPT2-carnitine palmitoyltransferase 2, PLIN3-perilipin 3, SOD1-superoxide dismutase 1, PGC1a-peroxisome proliferator-activated receptor gamma coactivator 1-alpha, RPL4-ribosomal protein L4*

The strongest effect on brain can be observed upon LCT/MCT diet and IF regimen in restbrain and hippocampus. Interestingly, genes for all metabolic pathways were up- or downregulated simultaneously. The pronounced upregulation of Gck in restbrain upon LCT/MCT has to be critically scrutinized given the lower expression of RPL4, which results in differences in the normalization offset of the ΔCt method. Nonetheless, we could also observe upregulation of Gck upon LCT/MCT in hippocampus and upon IF in restbrain, which showed stable mRPL4 expression levels. In cerebellum Gck was not quantifiable. We could further observe strong upregulation for SOD1 in restbrain upon LCT/MCT and IF. Interestingly, it was not higher expressed in hippocampus after LCT/MCT feeding, but significantly lower after CR like in hypothalamus and cerebellum. CACT and CPT1c were significantly upregulated in restbrain but not in hippocampus. PLIN3 showed again a higher expression in both regions. Indeed these effects are limited on restbrain and hippocampus. Hypothalamus and cerebellum showed generally another gene expression pattern. The strongest effects in these regions appeared upon CR. UCP4 was significantly lower expressed in cerebellum upon CR. However, in hypothalamus no significant changes in UCP4 expression could be observed (Fig. 3.5).

Although the plotted mean values seem to show metabolic adjustments in some cases the most part of them are not significant. Detailed data, showing statistical analysis as well, are shown in Fig. 3.7, 3.8 and 3.9.

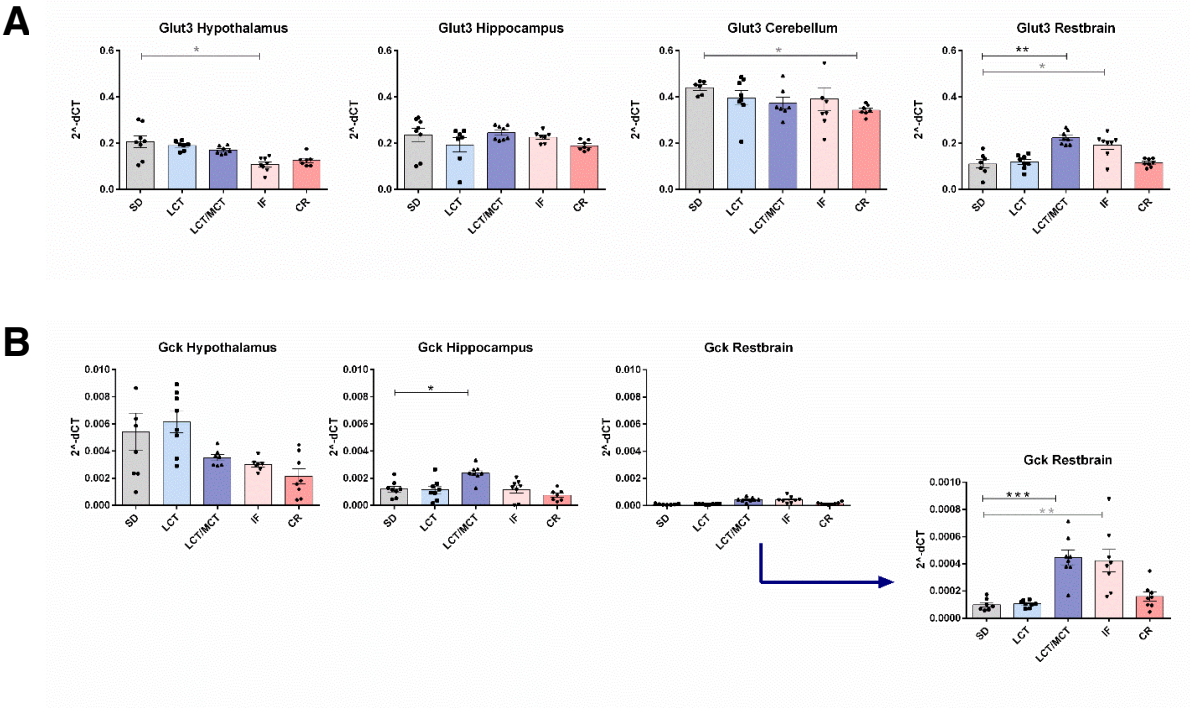


***Figure 3.7: mRNA expression of Glut3 and Gck representing the glycolytic pathway***

*(**A**) Relative mRNA levels of Glut3 normalized towards RPL4*

*(**B**) Relative mRNA levels Gck normalized to RPL4. Data for cerebellum are missing since expression was not quantifiable. Samples were analyzed in triplicates with n=8 biological replicates. Values are depicted as mean ± SEM. LCT, LCT/MCT, IF and CR were tested against SD respectively using one-way ANOVA, significant differences (P-values) marked with *P ≤ 0.05, ** P ≤ 0.01 and ***P ≤ 0.001.*

*$2^{-\Delta Ct}$-relative gene expression, SD-standard diet, LCT-long chain triglycerides, LCT/MCT-long and medium chain triglycerides, CR-caloric restriction, IF-intermitted fasting*

*Glut3-glucose transporter 3, RPL4-ribosomal protein L4, Gck-Glucokinase*

*(**C**) Correlation analysis of UCP4 to Gck (p=0.0001) in hippocampus. Each value in the graph corresponds to the sample of one mouse, with the abscissa indicating the expression of UCP4 and the ordinate indicating the expression of Gck. Based on the individual values, regression line was determined and is shown in the graph. Furthermore Pearson correlation coefficient (r) is given.*

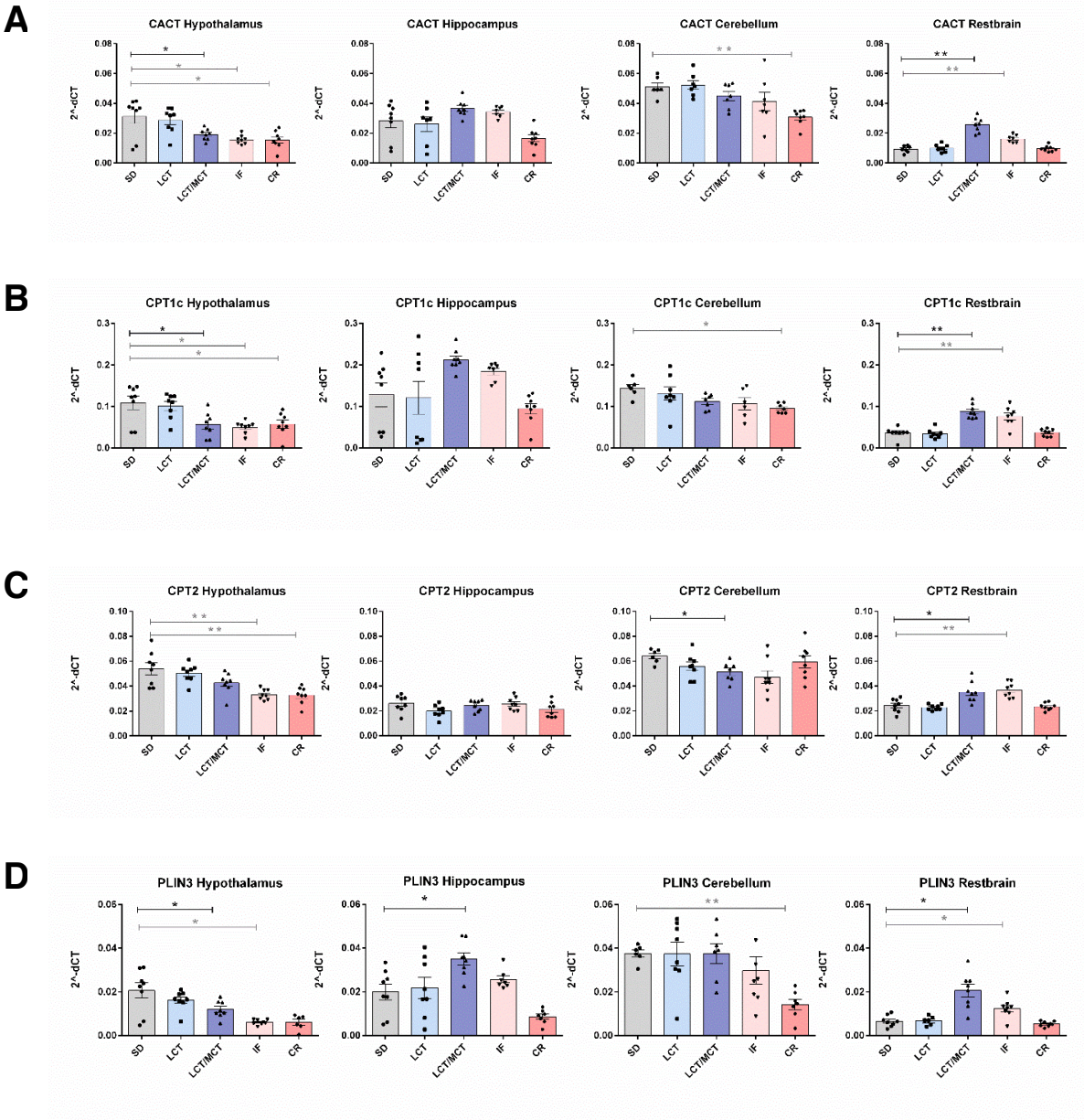


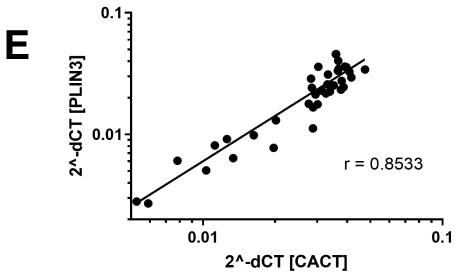


***Figure 3.8: mRNA expression of CACT, CPT1c, CPT2 and PLIN3 representing usage of FA***

*Relative mRNA levels of (**A**) CACT, (**B**) CPT1c, (**C**) CPT2, and (**D**) PLIN3 normalized to RPL4. Samples were analyzed in triplicates with n=8 biological replicates. The values are depicted as mean ± SEM. LCT, LCT/MCT, IF and CR were tested against SD respectively using one-way ANOVA, significant differences (P-values) marked with *P ≤ 0.05, ** P ≤ 0.01 and ***P ≤ 0.001. $2^{-\Delta Ct}$ - relative gene expression,*

*SD-standard diet, LCT-long chain triglycerides, LCT/MCT-long and medium chain triglycerides, CR-caloric restriction, IF-intermitted fasting, CACT-carnitin-acylcarnitin-transporter, CPT1c-carnitine palmitoyltransferase 1c, CPT2-carnitine palmitoyltransferase 2, PLIN3-perilipin 3*

(***E)*** *Correlation analysis of PLIN3 to CACT ($p<0.0001$) in hippocampus. Each value in the graph corresponds to the sample of one mouse, with the abscissa indicating the expression of CACT and the ordinate indicating the expression of PLIN3. Based on the individual values, regression line was determined and is shown in the graph. Furthermore Pearson correlation coefficient (r) is given.*

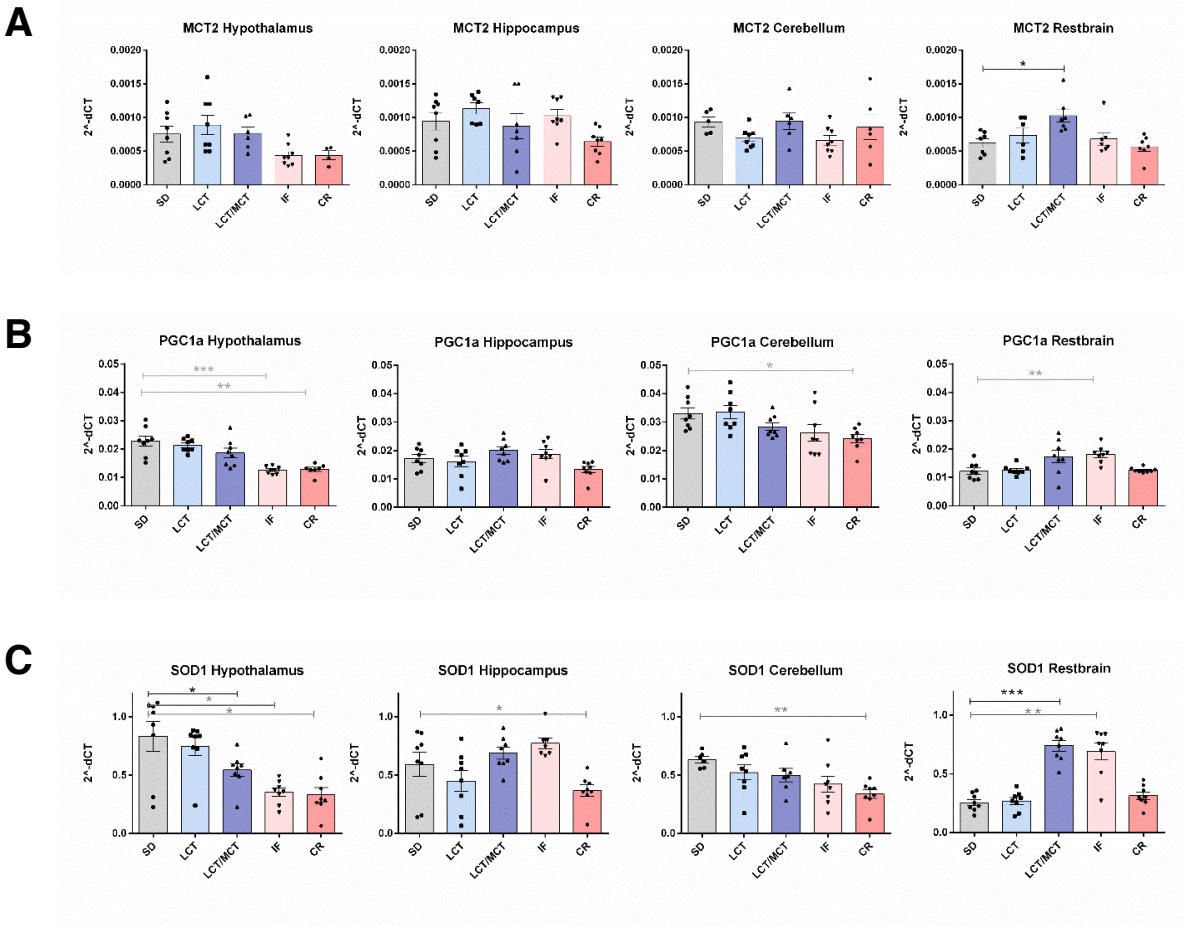


***Figure 3.9: mRNA expression of MCT2, PGC1a and SOD1 as important genes in ketogenesis***
*(**A)** Relative mRNA levels of MCT2 (**B)** PGC1a and (**C)** SOD1 normalized towards RPL4*
*Samples were analyzed in triplicates with n=8 biological replicates. The values are depicted as mean ± SEM. LCT, LCT/MCT, IF and CR were tested against SD respectively using one-way ANOVA, significant differences (P-values) marked with *P ≤ 0.05, ** P ≤ 0.01 and ***P ≤ 0.001.*
*$2^{-\Delta Ct}$-relative gene expression*
*SD-standard diet, LCT-long chain triglycerides, LCT/MCT-long and medium chain triglycerides, CR-caloric restriction, IF-intermitted fasting, MCT2-monocarboxylate transporter 2, PGC1a-peroxisome proliferator-activated receptor gamma coactivator 1-alpha, SOD1-superoxide dismutase 1, RPL4-ribosomal protein L4*

To investigate if all members of the shuttle system are regulated simultaneously, the relative expression of CPT1c and CPT2 ($2^{-\Delta Ct}$) of each mouse was compared with the corresponding expression of CACT ($2^{-\Delta Ct}$) in the same sample and plotted on a coordinate system (Fig. 3.10.). Each value in the graph corresponds to the sample of one mouse, with the X value indicating the expression of CACT and the Y value indicating the expression of either CPT1c or CPT2.

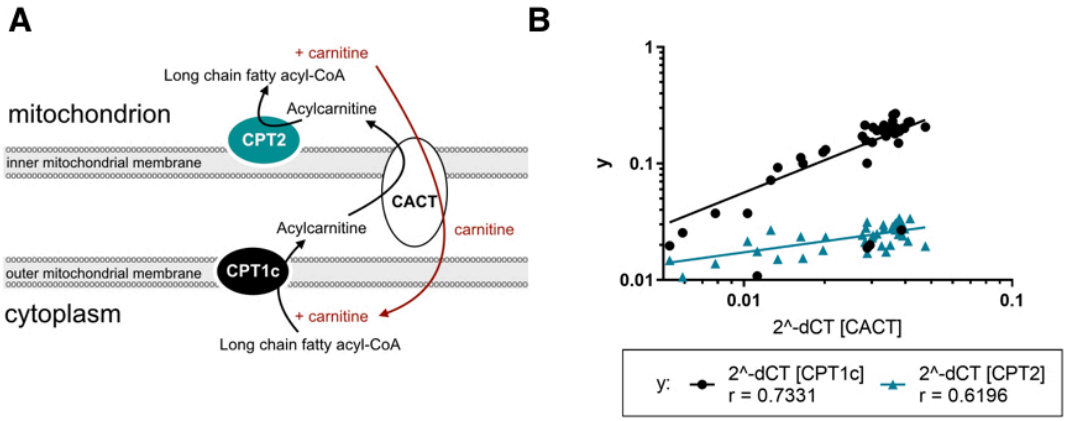


***Figure 3.10: Carnitine-acyltransferase system and its correlation of the gene expression in hippocampus***

*(**A**) schematic illustration showing the carnitine-acyltransferase system which is responsible for FA transport over the mitochondrial membrane (modified from Ceccarelli et al. 2011) CACT-carnitin-acylcarnitin-transporter, CPT1c-carnitine palmitoyltransferase 1c, CPT2-carnitine palmitoyltransferase 2*

*(**B**) Correlation of CPT1c and CPT2 gene expression with CACT gene expression were analyzed within the hippocampus. The abscissa indicates the gene expression($2^{-\Delta Ct}$) of CACT and the ordinate the gene expression of either CPT1c or CPT2 respectively. Based on the individual values, the regression line was determined and is shown in the graph. The Pearson correlation coefficient r was determined using correlation analysis.*

Correlation analysis of CPT1c and CPT2 to CACT showed that CPT1c (r=0.7331) and CPT2 (r=0.6196) gene expression correlates significantly with expression of CACT (both $P \leq 0.001$) .(Fig. 3.10). However, it can be observed that expression of CPT1c increases more in relation to CACT than expression of CPT2.

We further compared CACT gene expression to PLIN3 gene expression (Fig.3.8 E) and could show a significant correlation of these two genes ($p<0.001$, $r=0.8533$). Since an overlap of UCP4 and Gck was considered (Liu et al. 2006) we repeated correlation analysis in the same way for the expression of these two genes (Fig.3.7 C) and found them to correlate significantly ($p=0.0001$, $r=0.5866$) as well.

## 3.4 Relationship between brain regions, cell type and UCP4 protein expression

Western Blot analysis was used to investigate the expression of UCP4 at protein level. We determined the proportions of different brain cells, such as neurons, astrocytes and microglia in the four different regions hypothalamus, hippocampus, cerebellum and restbrain, in order to compare them in the next step with the distribution of UCP4 in the brain. For every region samples from 5 different mice of the standard diet group were included in the experiment. The samples were taken from the second feeding trial in 2021(ii). On every membrane inclusion bodies containing recombinant UCP4 and two different brain standards consisting of the whole brain were loaded as positive controls and a spleen standard as a negative control. The intensity values of each animal were normalized either towards ß-actin as a housekeeping gene or mitochondrial markers (VDAC, SDHA and OGDH) and the average of both brain standards.

The data shows that UCP4 protein expression normalized to ß-actin in the hypothalamus is higher compared to the brain standard ($i_x/i_0=1$), which is a protein lysate of the whole brain. In contrast, slightly lower levels of UCP4 expression can be reported in hippocampus and cerebellum, whereas restbrain does not differ significantly.

Normalization to all of the four reference proteins (see chapter 2.2.12) shows that the amount of UCP4 is lowest in cerebellum and the highest in hypothalamus (Fig. 3.11, A-D). In hippocampus the relative abundance of the protein varies. Importantly, the relative amount of protein in the five biological replicates of each brain region did not differ greatly, resulting in better validity of the data despite the small number of samples per group.

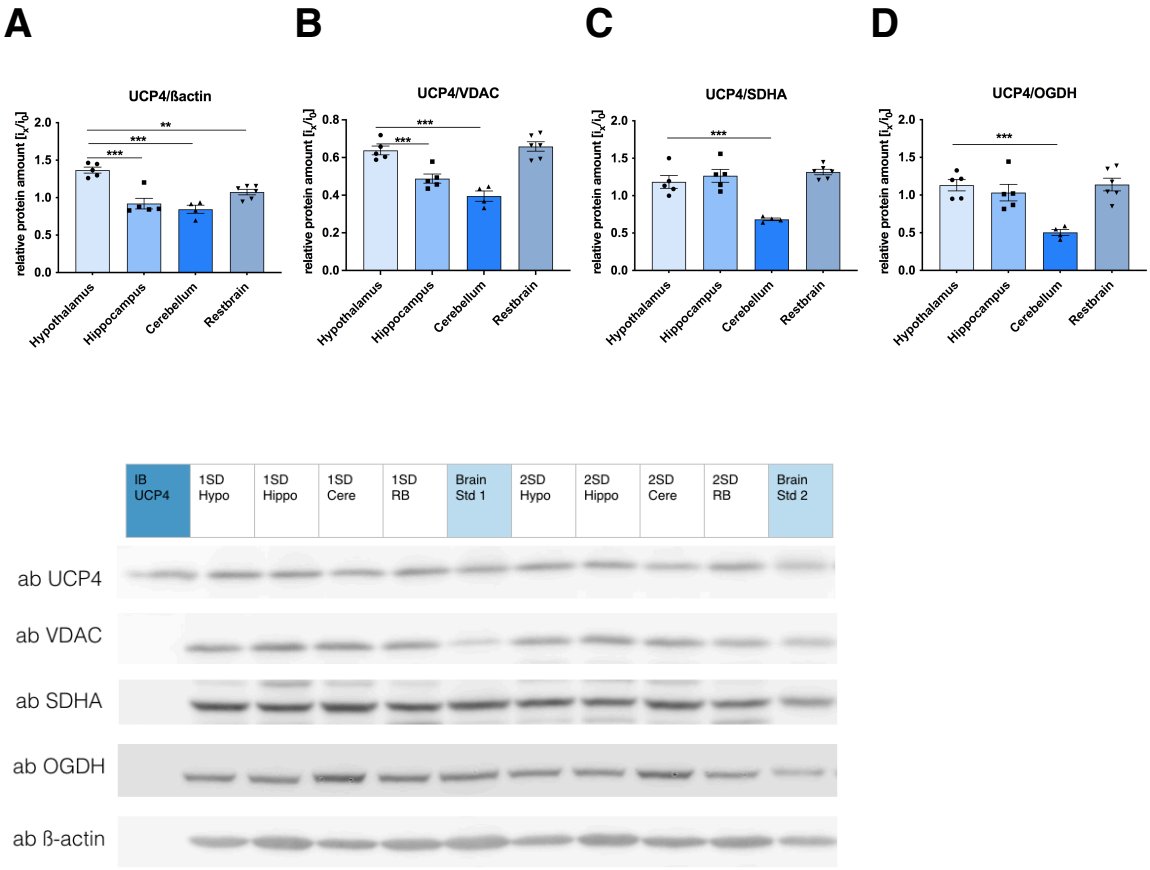


***Figure 3.11: Comparison of UCP4 protein levels in different regions of the central nervous system***

*Protein levels are presented as ratios of UCP4 to either (**A**) ß-actin as a housekeeping protein or (**B**) VDAC, (**C**) SDHA and (**D**) OGDH as mitochondrial markers ($i_x$) and normalized to the mean of this ratio in two brain standards ($i_0$). For statistical analysis hippocampus, cerebellum and restbrain are compared to hypothalamus using a one-way ANOVA, n=5, Values are depicted as mean values ± SEM, *P ≤ 0.05, ** P ≤ 0.01 and ***P ≤ 0.001. (**E**) Representative Western Blot showing UCP4 protein expression compared to the expression of mitochondrial markers and ß-actin as a housekeeping gene in different brain regions. Tissue samples derived from the SD group. Gels were loaded with 20µg total protein per lane. UCP4 inclusion body and two different brain standards were used as a positive control.*

*VDAC-voltage dependent anion channel, SDHA-complex II, OGDH-oxoglutarate dehydrogenase hippo-hippocampus, cere-cerebellum, RB-restbrain, hypo-hypothalamus*

Since mitochondrial amount and morphology can differ between tissue and cell types (Fernández-Vizarra et al. 2011) and vary in dependence on external conditions (Wai and Langer 2016, Cogliati et al. 2016 ) we used proteins localized in different parts of the mitochondrion. VDAC is a protein abundant in the outer mitochondrial membrane, whereas SDHA (succinate dehydrogenase complex, also known as complex II of the electron transport chain) can be found in the inner mitochondrial membrane. OGDH is a mitochondrial matrix protein of the TCA cycle. Fig. 3.12 shows the protein expression of each mitochondrial protein normalized to ß-actin.

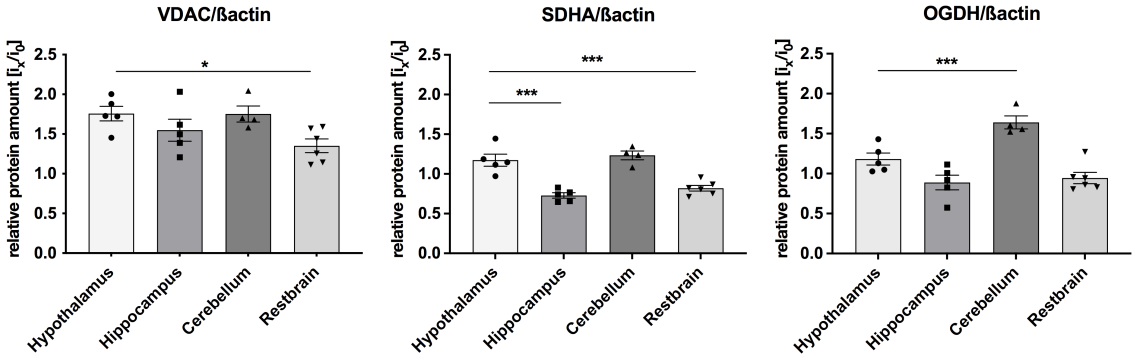


***Figure 3.12: Comparison of three mitochondrial marker proteins representing outer mitochondrial membrane (VDAC), inner mitochondrial membrane (SDHA) and mitochondrial matrix (OGDH)***

*Protein levels of VDAC, SDHA and OGDH were presented as ratios to ß-actin ($i_x$) and normalized to the mean of this ratio in two brain standards ($i_0$). For statistical analysis hippocampus, cerebellum and restbrain were compared to hypothalamus using a one-way ANOVA, n=5. Values are depicted as mean values ± SEM, *P ≤ 0.05, ** P ≤ 0.01 and ***P ≤ 0.001.*
*VDAC-voltage dependent anion channel, SDHA-complex II, OGDH-oxoglutarate dehydrogenase*
*A representative Western Blot is shown in Figure 3.10*

Interestingly, differences in protein expression of complex II and OGDH in the different brain regions can be observed (Fig. 3.12). While these two mitochondrial proteins are significantly more present in the hypothalamus and cerebellum less pronounced but similar differences of VDAC can be detected. Although the mitochondrial quantity cannot be estimated exactly, the distribution of these three proteins may indicate a slightly higher number of mitochondria in the hypothalamus and cerebellum. However, since these effects could also occur in as a

result of variations in the ß-actin levels, analysis of other housekeeping proteins would be required to confirm these suggestions.

## 3.5 UCP4 expression in astrocytes

It was previously discussed whether UCP4 can also be assigned to astrocytes in addition to neurons (Smorodchenko et al. 2009, Perreten Lambert et al. 2014). To check this, lysates of sorted cells, either neurons, astrocytes or microglia, obtained by a cooperation partner (M. Maes, IST, Klosterneuburg, Austria) and from us were analyzed by Western Blot. SDHA and ß-actin as loading controls and glial fibrillary acidic protein (GFAP) and ionized calcium-binding adapter molecule 1 (IBA1) to check the purity of the samples.

Our results support the already described abundance of UCP4 in astrocytes (Smorodchenko et al. 2009). However, quantification of the bands and normalization to ß-actin yielded the UCP4 amount in astrocytes to be just 1,9% of the amount observed in neurons. Expression of UCP4 protein in microglia cannot be registered (Fig. 3.13). The absence of GFAP in microglia indicates a high purity of this sample. Since no UCP4 protein could be detected in microglia, the portion of UCP4 protein in the astrocytes samples can most likely be just be attributed to astrocytes themselves, although the presence of IBA1 indicates that these samples also contained a small amount of microglia.

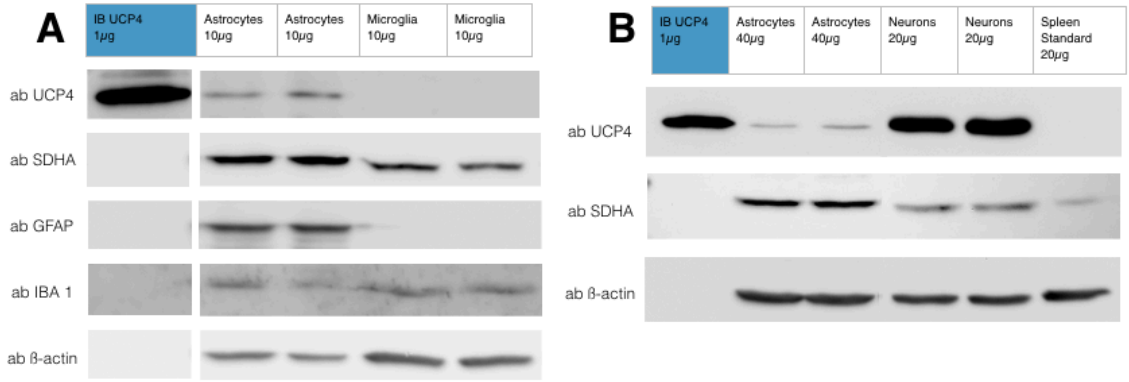


***Figure 3.13: Representative Western Blot showing UCP4 protein amount in neuronal and glial cells.***

***(A)*** *qualitative comparison of UCP4 protein amount in murine astrocytes and microglia and* ***(B)*** *astrocytes to neurons using anti-UCP4 antibody. 10-40 µg of cell lysates (astrocytes, neurons and microglia) were loaded per lane. UCP4 inclusion body (IB UCP4) was used as a positive and spleen standard as a negative control for UCP4 protein.*
*SDHA- complex II, GFAP-glial fibrillary acidic protein, IBA1-Ionized calcium-binding adapter molecule 1*

## 3.6 Distribution of cells among different brain regions

To check whether the differences of UCP4 protein expression can be assigned to differences of the most abundant cell type in each region, expression of cell specific proteins was compared. Neuronal nuclei (NeuN) was used as neuronal, GFAP as astrocytic and IBA-1 as microglial marker. A representative Western Blot is shown in figure. 3.14 E.

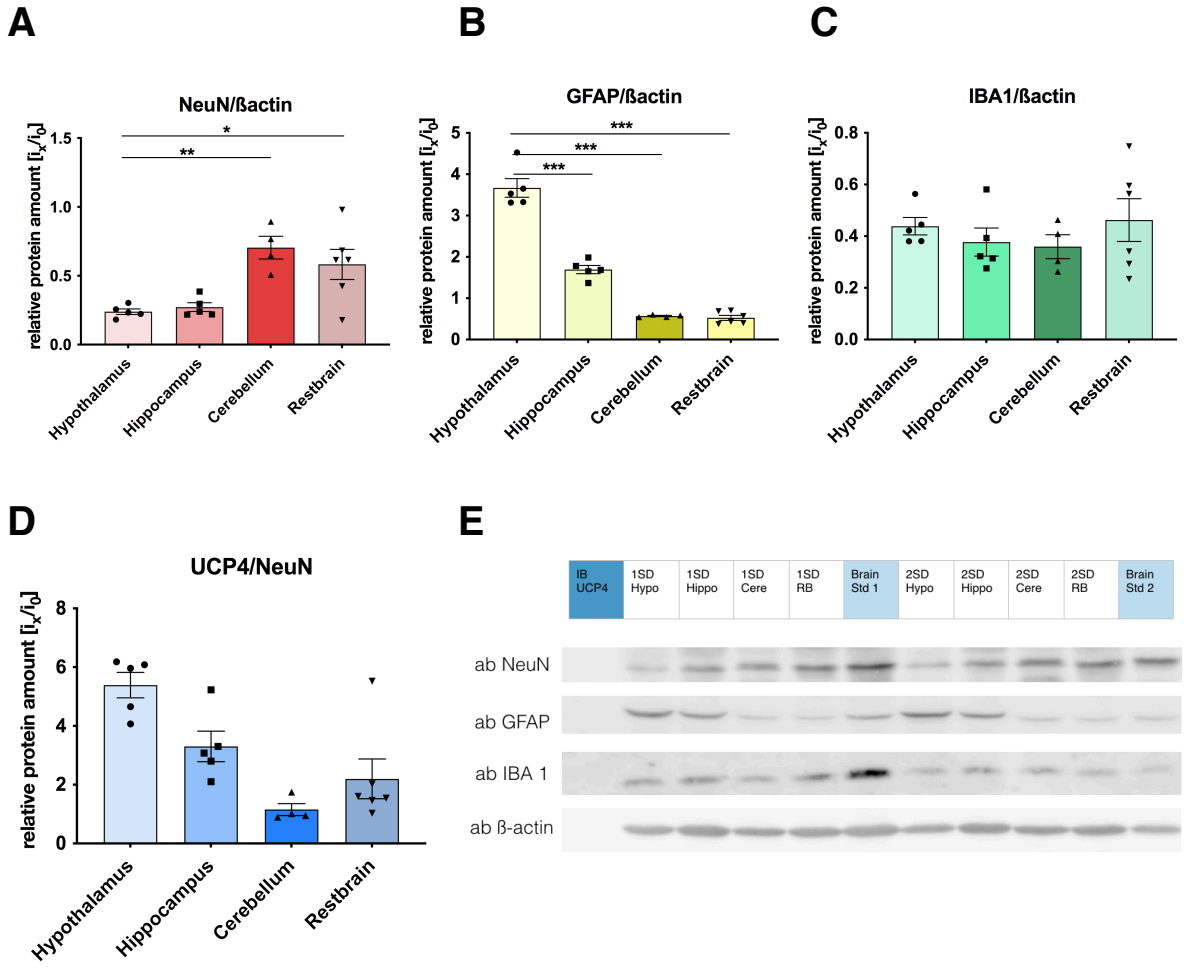


***Figure 3.14: Distribution of neuronal and glial cells within different brain regions***
*Protein levels are presented as ratios of the distinct marker proteins for (**A**) neurons (NeuN), (**B**) astrocytes (GFAP) and (**C**) microglia (IBA1) to ß-actin ($i_x$) respectively normalized to the mean of this ratio in two brain standards ($i_0$). (**D**) Ratio of UCP4 to NeuN normalized to brain standard. For statistical analysis hippocampus, cerebellum and restbrain were compared to hypothalamus using a one-way ANOVA, n=5. All values are depicted as mean values ± SEM, *P ≤ 0.05, ** P ≤ 0.01 and ***P ≤ 0.001 (**E**) Representative Western Blot showing NeuN, GFAP and IBA-1 protein expression in different brain regions. Tissue samples derived from the SD group. Gels were loaded with 20µg total protein per lane. UCP4 Inclusion body and two different brain standards were used as a control NeuN-neuronal nuclei, GFAP-glial fibrillary acidic protein, IBA1-Ionized calcium-binding adapter molecule 1, hippo-hippocampus, cere-cerebellum, RB-restbrain, hypo-hypothalamus*

Since we have selected only one marker protein for each cell population, these Western blots just give us an idea of the distribution of the cells.

Western Blot analysis demonstrated that the relative amount of the neuronal marker (NeuN/ ß-actin) is higher in the cerebellum and restbrain. However, the individual values for each mouse vary in these regions more widely. These results correspond to the qualitative representation of the distribution of neurons by nissl-staining of a sagittal section of the whole brain (Fig. 2.2)

Furthermore, quantitative analysis showed that the astrocytic marker (GFAP) is highly abundant in the hypothalamus but also the hippocampus showed an approximately two-fold amount of GFAP expression compared to cerebellum or restbrain. These two regions showed less GFAP expression than the brain standard, since relative protein amount is less than 1.

Previous studies (de Haas et al. 2008, Mittelbronn et al. 2000) revealed differences in local distribution of microglia, without involvement of inflammatory processes. This we could not observe (Fig. 3.14 C) with our experimental setup, using IBA1 as a marker protein for microglia. Further investigations with more proteins representing each cell type are needed at this point to confirm or deny these local differences.

Fig. 3.14 D shows the proportion of UCP4 protein along the neurons of the four brain regions. This is an idealized representation, since the very small proportion of UCP4 protein, attributable to astrocytes (Fig. 3.13), is not taken into account. This graph suggests a higher amount of UCP4 in neurons of the hypothalamus than in other regions, although the single values spread more widely.

## 3.7 Influence of different dietary interventions on the expression of UCP4 protein in mouse hypothalamus, hippocampus, cerebellum and restbrain

To check the changes in UCP4 mRNA expression due to different dietetic conditions on protein level Western Blots were performed (Fig. 3.15). Western Blot analysis did not reveal significant changes in UCP4 protein expression upon different feeding regimens. All of the Western Blots showed a relatively high variation in UCP4 protein expression especially in the hippocampus. These distribution patterns were the same when normalizing to VDAC instead of $\beta$-actin (Suppl. Fig. 3).

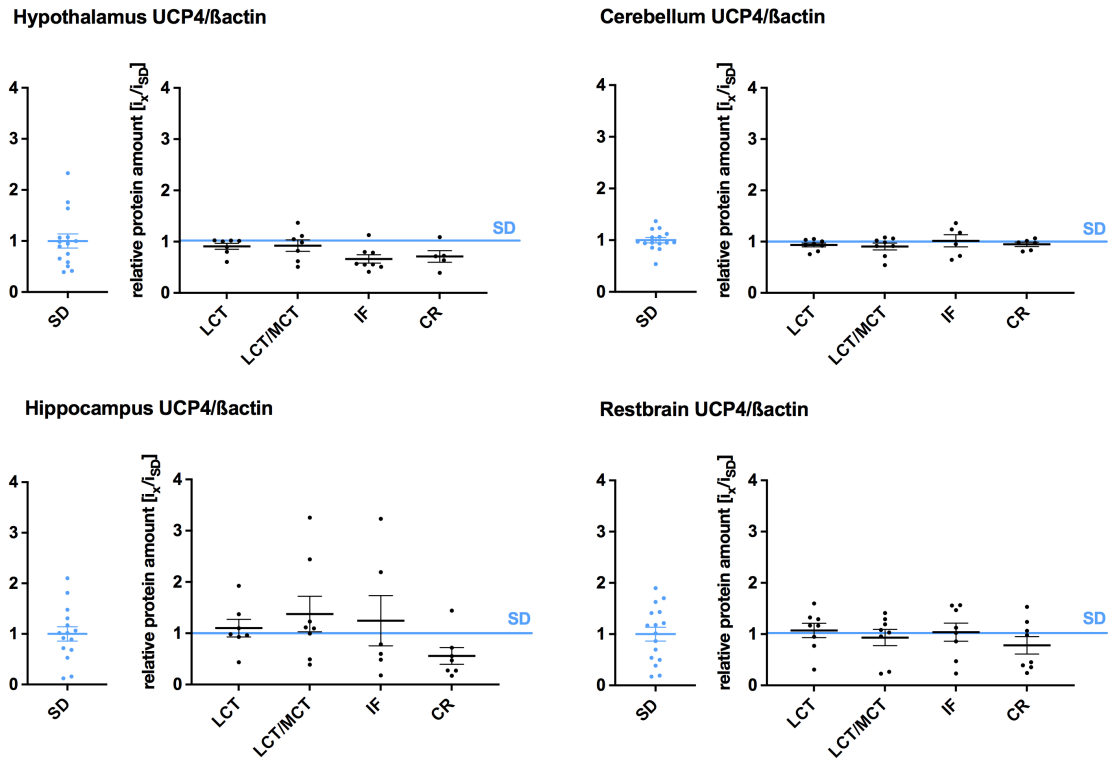


***Figure 3.15: UCP4 protein expression of the different brain regions of mice fed with KDs and fasting regimen***

*20µg protein lysate of eight animals per diet were loaded on Western Blot. All samples of IF and CR originated from 2019, whereas SD, LCT and LCT/MCT group include four samples from 2019 and 2021 respectively (n=8)*

*Protein levels are presented as ratios of UCP4 to ß-actin ($i_x$) which were detected on the same membranes consecutively and normalized towards the SD ($i_{SD}$), which was set to 1. The values are presented as mean± SEM. A representative Western Blot is shown in the supplementary data.*

*SD-standard diet, LCT-long chain triglycerides, LCT/MCT-long and medium chain triglycerides, CR-caloric restriction, IF-intermitted fasting*

Finally, we investigated whether different dietetic regimes can influence the expression of other mitochondrial proteins in brain. Therefore, we determined the amount of VDAC and SDHA as a ratio to the amount of b-actin. We could not observe any changes in the expression of these two proteins among different dietetic regimes.

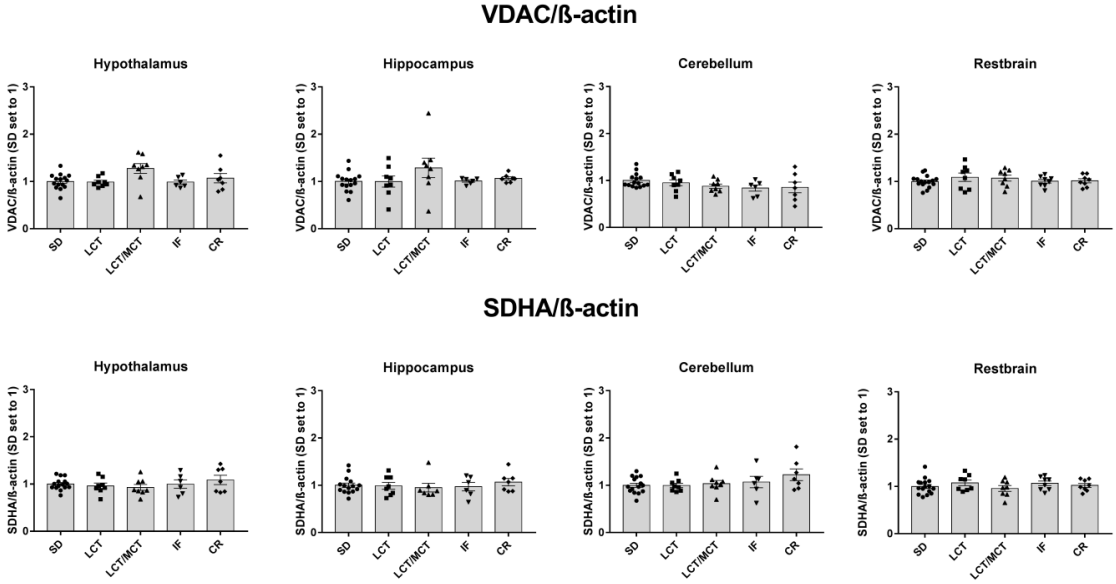


***Figure 3.16: VDAC and SDHA protein expression of the different brain regions of mice fed with KDs and fasting regimen***

*Protein levels are presented as ratios of either VDAC or SDHA to ß-actin and normalized towards the standard diet, which was set to 1. The values are presented as mean± SEM, n=8. Statistical analysis revealed no significant differences.*

*SD-standard diet, LCT-long chain triglycerides, LCT/MCT-long and medium chain triglycerides, CR-caloric restriction, IF-intermitted fasting, VDAC-voltage dependent anion channel, SDHA-complex II.*

*A representative Western Blot is shown in supplementary data.*

# 4. Discussion

This study was performed based on methods previously validated by pre-tests. It was shown that the RNA isolation method is suitable for RNA from brain tissue (see chapter 3.1). The primers were designed specifically for these experiments and their efficiency was confirmed by appropriate testing (see chapter 3.2). For the analysis of protein expression, a new charge of a specific anti-UCP4 antibody was produced and validated (see chapter 2.2.13 and Suppl. Fig. 5).

Through our experiments, we could observe higher UCP4 mRNA expression in hippocampus upon the KD (ratio of fat: carbohydrate+protein = 8:1) containing both LCT and MCT but not in the other one which just contained LCT, and lower expression in the cerebellum in CR fasting regimen with RT-qPCR. However, the UCP4 gene expression did not correlate with the protein expression in the present study. Furthermore, we could confirm and quantify proposed differences of UCP4 protein levels among distinct brain regions using a self-designed and evaluated antibody (Smorodchenko et al. 2009). We have compared the levels of UCP4 with the presence of neuronal and glial cell populations to obtain first indications of the distribution of UCP4 in different cell types and brain regions. We analyzed levels of UCP4 protein in cell lysates of neurons, astrocytes and microglia. Our findings suggest that UCP4 protein is mainly attributed to neurons. Astrocytes contain only around 2% of neuronal UCP4. This supports the previous results, showing UCP4 as mainly occurring in neurons (Smorodchenko 2009, Smorodchenko 2011) and contradict the reports on high abundance of UCP4 in astrocytes in vitro (Perreten Lambert et al. 2014).

PCRs are very sensitive to even very small changes in gene expression.The results of our gene expression analyses by RT-qPCR suggest that diets may have an impact on the presence of UCP4. Despite the sometimes very high variability within the groups, statistically significant differences can be found. The extent of regulation of UCP4 gene expression was dependent on the type of KD, the respective fasting conditions and the specific brain region. In general the strongest effects can be observed upon LCT/MCT diet and IF regimen in restbrain and hippocampus. There, expression of UCP4 and genes involved in FA metabolism, but also glucose metabolism, such as PLIN 3 or Gck, showed significant upregulation. In contrast, the most striking effects in the cerebellum occurred upon CR, where UCP4 and genes involved in FA metabolism, like CACT, CPT1c and PLIN3, but also PGC1a and SOD1 were significantly lower expressed than in the SD. In the Hypothalamus no significant changes in UCP4 expression can be observed. Since the biological replicates

for some groups are sometimes highly variable, one should consider the metabolic situation of each animal at the end of the feeding trial. Especially in the fasting groups (IF and CR), where food was not offered ad libitum, there might be differences between alpha and omega animals concerning their feed intake, resulting in weight differences. In turn, normal or overweight animals do not develop ketosis, metabolism does not need to be adjusted, and they will bias the results of the group. Therefore it might be interesting to additionally correlate the obtained data to the changes of the animals body weight.

It already has been suggested, that KDs may affect the expression of UCP4. Using immunobloting Sullivan et al. (2004) observed an enhanced UCP2, UCP4 and UCP5 expression in hippocampus of mice after one and a half weeks of 6:1 KD feeding regime (Sullivan et al. 2004). Our animals were fed the 8:1 KDs over eight weeks. Interestingly, we observed similar changes in UCP4 mRNA expression in hippocampus but not at protein level. In this case our Western Blot results, which did not show differences between SD and both KDs (Fig. 3.15), can be considered more precise, since we used a self-designed UCP4-antibody (Smorodchenko et al. 2009), which is more specific than commercial ones used in Sullivan et al. 2004. We additionally loaded UCP4-containing inclusion bodies as a positive control to check the specificity of our anti-UCP4 antibody. However, we cannot conclude that there are definitely no changes in protein expression, since Western blots are generally much less sensitive than PCRs for methodological reasons. Systematic errors may occur at many points in the process. Examples can include voltage fluctuations during transfer, changes in environmental conditions such as room temperature affecting antibody binding, or manual selection of ROIs during quantification. This could mean, that we just couldn't visualize very minimal changes at this point.
Sullivan et al. (2004) discussed the increased proton leak and reduced amount of ROS, which they observed in hippocampus upon KD, to be a result of upregulation of uncoupling proteins. However, since they reported UCP2 and UCP5 protein to be increased as well, these effects cannot be assigned to all of the three UCPs including UCP4 for certain. Interestingly, the previous results of Pohl`s group showed no UCP5 at protein level in brain, neither under physiological conditions (Smorodchenko et al. 2009, Smorodchenko et al. 2011) nor by inflammation (Smorodchenko et al. 2017). Also UCP2 was found to be expressed only in microglia cells (Rupprecht et al. 2012).
We observed an increase of UCP4 mRNA expression in hippocampus and restbrain due to the dietary supplementation of one-third MCTs. This is surprising assuming the hypothesized dual function for UCP4 like proposed for UCP3. Hereby the uncoupling proteins would also have FA-transporting functions (Pohl et al. 2019). MCFAs in contrast to LCFAs can pass the

inner mitochondrial membrane passively, as they do neither require cytoplasmatic fatty acid binding proteins nor carnitine (Schönfeld and Wojtczak 2016). Because of this, we expected the carnitine-acyltransferase system members CACT, CPT1c and CPT2 to be higher expressed in a diet containing only LCTs. But again, parallel to UCP4 expression, we only observed a significant upregulation of CACT and CPT1c ($P \leq 0.01$) upon IF in restbrain. However, CPT2 is not affected. This coincides with literature, which characterizes just CPT1 isoform expression and activity level to be dependent on multiple factors like metabolic state, cold or infections (Ceccarelli et al. 2011). Brain CPT1c is furthermore involved in fatty acid synthesis through buffering of malonyl-CoA (Ceccarelli et al. 2011). Falling levels of malonyl-CoA in the liver activate CPT1, resulting in higher transport activity of fatty acids and ketogenesis (McGarry and Foster 1979). At this point it would be interesting to know to which part LCT and MCT contribute at FAO compared to ketogenesis, since another explanation of the increased expression of several genes in hippocampus and restbrain upon LCT/MCT feeding might be the fact that octanoate itself, as a medium chain fatty acid can stimulate ketogenesis (Thevenet et al. 2016). Glycolysis is reduced, resulting in a low cytosolic NADH+/NAD+ ratio, which leads to activation of SIRT and PGC1a subsequently (Lagouge et al. 2006). Recently, Wang et al. reported such an upregulation of PGC1a upon MCT diet, parallel to an upregulation of its upstream activators AMPK, AKT and mTOR in skeletal muscle (Wang et al. 2018). However, our results did not show any upregulation of PGC1a upon KDs or fasting regimen except in restbrain after IF ($P \leq 0.01$).

We have not analyzed genes whose expression can be related to the number of mitochondria like VDAC with qPCR, although this would be important to certainly exclude the possibility that the changes of UCP4 and other mitochondrial genes are balanced relative to the number of mitochondria. Nevertheless we investigated VDAC and SDHA on protein level, where we could not observe changes in protein level upon the different diets. This is interesting since there is already a controversial reports about a rising amount of mitochondria upon KD in brain (Bough et al. 2006), whereas recent studies reported the contrary in heart (Xu et al. 2021).

Apart from the changes upon the KDs, we observed an increased UCP4 expression in restbrain under IF and a decreased expression under caloric restriction in cerebellum. Genes corresponding to the different metabolic pathways of glycolysis or usage of FA in brain were slightly regulated in the same direction as UCP4 in each diet and region respectively. Thereby even the lipid handling protein PLIN3 was affected by the different diets and its expression in hippocampus correlated significantly with CACT ($r=0.8533$). Hilse et al. suggested interactions between lipid droplets (LDs)-mitochondria and UCP3 in heart. Literature never discussed such an interaction for UCP4 in brain before, because they were

thought not to be present in the brain (Schönfeld and Reiser 2013). Recently, Alzheimer's disease risk-gene ApoE4 was shown to decrease sequestration of FA in LDs in Astrocytes in vitro (Qi et al. 2021) and in vivo LDs are reported especially in the hypothalamic area (Maya-Monteiro et al. 2021). However, LDs were found to be co-localized with IBA1 in brain, which indicates UCP2 expressing microglia to be the main storage of LDs, although other studies showed several cell types of the brain including neurons to be able to form LDs (for review see Farmer et al. 2020). In order to draw conclusions about possible interactions of UCP4, similar to those of UCP3, in the brain, further experiments would be necessary.

In restbrain IF but not CR leads to similar changes as LCT/MCT. The fact that fasting results in ketogenesis as well, and thereby initiates the same regulation processes is well known (Wallace et al. 2010), but our results indicate that IF might be more effective to promote changes in metabolism than CR.

Although a ketogenic state is classified by almost no metabolisation of glucose, we observed a simultaneous increase of genes encoding proteins of the glycolytic pathway like glucokinase as well in hippocampus and restbrain. A correlation analysis of UCP4 and glucokinase expression data in the hippocampus revealed a significant (P=0.001) correlation (r=0.5866). Glucokinase is the rate-limiting enzyme of the glycolytic pathway and was already considered to overlap with UCP4 by Liu et al. (2006).They reported UCP4 to protect cells against the collapse of energy supply through FCCP, which uncouples mitochondrial respiration. They assigned this protective role to the ability of UCP4 to shift the metabolism towards glycolysis, where ATP is produced independent of mitochondrial respiration. They furthermore observed a higher glucose uptake due to UCP4 expression. This concurs with the upregulation of GLUT3, which we noticed in restbrain upon LCT/MCT and IF. Of course these results have to be discussed critically, since Liu et al.(2006) used UCP4 transfected pheochromocytoma cells in vitro, while we worked with an in vivo model of the brain. We can only speculate that regions, where we saw upregulation of glucokinase are highly dependent on glucose, so that they are also supplied with glucose even in the state of starvation. The region specific effects cannot be explained through differences in blood-perfusion, therefore another explanation could be alterations in the anatomy of the blood-brain barrier. This is already described for the blood-brain barrier at the arcuate nucleus of hypothalamus, which is more permeable for nutrients (Haddad-Tóvolli et al. 2017). Highly specialized nutrient-sensing neurons in this area physiologically modify the metabolic response of the whole body to nutrient availability (Le Foll 2019). Interestingly UCP4 mRNA expression was reported to be highly expressed in this distinct hypothalamic area (Liu et al. 2006). This is in line with our results, which showed the UCP4 protein level in the whole hypothalamus to be the highest amongst the investigated regions.

Although we observed alterations in UCP4 gene expression, Western Blot analysis revealed no changes on protein level upon different diets.
Our present results question the role of UCP4 as a metabolically active protein and support the idea that long-lived proteins like UCP4 cannot be involved in fast-adapted processes like energy homeostasis. However, protein turnover of most brain proteins ranges from one day to a few weeks (Fornasiero et al. 2018), the classification as a long-lived protein indicates an even longer time until UCP4 is degraded and exchanged. Possibly the setup of the feeding trial was too short to see effects of UCP4 regulation on protein level as well. Furthermore, we lack the information, whether the metabolic state of ketogenesis can be confirmed on protein level in the specific brain regions. Therefore investigation of protein levels of specific indicators for ketogenesis like AMPK will be necessary.

Literature presented a divergent description of UCP4 amount in different brain regions at mRNA and protein levels. Although Liu et al. reported that the highest UCP4 mRNA expression could be found in hippocampus, the qualitative Western Blots in the same study (Liu et al. 2006) have shown that cortex and hypothalamus have higher UCP4 protein levels than hippocampus. Smorodchenko et al. (2009) quantified UCP4 protein levels in cortex, cerebellum brainstem and spinal cord using immunoblot and found the highest UCP4 amounts in cortex. Our present results revealed the highest amount in hypothalamus followed by restbrain, which mainly consists of cortex but also includes thalamus and amygdala amongst others. These region specific expression patterns of UCP4 correspond to the preferential expression of UCP4 in neurons described by Smorodchenko et al. (2009). Contrary to that we detected the least neuronal marker NeuN in hypothalamus, where the highest levels of UCP4 were detected, whereas the NeuN/ß-actin ratio was the highest in cerebellum, where the lowest levels of UCP4 normalized to ß-actin could be observed. Thus the ratio of UCP4 to NeuN is much higher in hypothalamus than in cerebellum (Figure 3.14 D). However, it should be taken into account that NeuN doesn´t detect some fractions of neurons such as Purkinje cells and dentate nucleus neurons of the cerebellum (Mullen et al. 1992). This might draw a misleading picture, since we can assume that the amount of neurons in the cerebellum is higher than depicted whereby the ratio of UCP4 to NeuN is getting even lower in cerebellum compared to other regions. For mouse, literature describes the cerebellum to contain 60% of total brain neurons (Herculano-Houzel 2010).
We observed that the proportion of astrocytes, represented by GFAP, is the highest in hypothalamus followed by hippocampus (Fig. 3.14B). We further compared the line intensity of UCP4 bands from astrocytes and neurons with the result that neurons have about 50-fold more UCP4 (Fig. 3.13). Given this fact, we were could disregard the negligible fraction of

astrocytic UCP4 in the plot of UCP4/NeuN (Fig. 3.14D), although GFAP is about 4-fold higher in hypothalamus than in cerebellum (Fig. 3.14B). We conclude, that UCP4 protein levels differ among neuronal populations, which in turn have to be explained through region-specific demands, and these specific demands are not uncovered completely yet. Additionally, cell populations such as neurons and astrocytes are characterized by only one marker protein in this study, instead of two or more, providing only an indication, but not a definitive statement of the occurrence of each cell type, as each protein is subject to some variation. Further studies should focus on immunofluorescence staining on tissue slices to clarify the exact distribution of UCP4 among the cell populations and different neuronal subtypes in the different brain regions.

## 5. Outlook

Although we could show a specific UCP4 protein distribution amongst several brain regions and some effects of different feeding regimens on UCP4 mRNA expression, no clear picture about its distinct function in neuronal metabolism emerges so far. We now suggest that differences in protein expression of UCP4 among brain regions may be explained by different neuronal cell type ratio, specific metabolism or electrical activity of brain structures. Further experiments are required to further investigate these hypothesis. Since we previously just analyzed whole tissue lysates for UCP4 and obtained an idea about its distribution, it may now be interesting to sort cells from the different brain regions after a feeding experiment to specifically assign the presence of UCP4 to a cell population and detect changes in its amount. Another option could be immunofluorescence to colocalize UCP4 with neuronal populations.

## 6. Abstract

Uncoupling protein 4 (UCP4) belongs to the solute carrier family (SLC25) and is highly abundant to the inner mitochondrial membrane of neurons and at significantly lower levels in astrocytes. So far, none of the UCP4´s physiological functions, proposed based on its putative proton transport function and homology to UCP1, such as thermogenesis, regulation of ROS or calcium homeostasis, or involvement in cell differentiation and apoptosis, could be convincingly demonstrated. Some previous studies observed an adaptive shift in energy metabolism through UCP4 expression. Recent reports also suggest that other UCP family members (UCP2 and UCP3) functions as dual transporters for protons and substrates and their expression correlates with the cell metabolism. Therefore, we hypothesized that UCP4 could be important for the metabolic flexibility of neurons. In this work, we aimed to test whether (i) UCP4´s expression is altered upon prolonged changes in nutrient availability, and (ii) UCP4 protein amount differs regionally in the brain due to the different metabolic activity and anatomical structure of the distinct brain regions.

For this we analyzed UCP4 gene and protein expression levels in mice, obtaining (A) high-fat ketogenic diets such as long-chain triglycerides (LCT) or long- and medium-chain triglycerides (LCT/MCT), or (B) fasting regimens such as intermittent fasting (IF) and calorie restriction (CR).

We detected that UCP4 mRNA but not protein levels were higher in the hippocampus after eight weeks of LCT/MCT diet, and animals fed CR showed lower levels of *ucp4* expression in the cerebellum. However, we didn´t observe any relevant changes in UCP4 protein expression at different feeding regimes, suggesting no correlation between these parameters under our experimental conditions..

Interestingly, we found different UCP4 protein levels among brain regions with the highest UCP4 amount in the hypothalamus and the lowest - in the cerebellum. We also confirmed the previous results that UCP4 is present in astrocytes, but at a much lower level than in neurons.

The absence of diet-dependent changes on UCP4 protein expression in our model suggests that we cannot attribute the beneficial effect of dietary interventions in preventing and impeding the progression of neurodegenerative diseases to the UCP4 function.

# 7. Zusammenfassung

UCP4 ist ein Protein, welches sich vor allem in der inneren mitochondrialen Membran von Neuronen, aber in geringeren Mengen auch in Astrocyten befindet und zur Familie der „Solute carrier proteins“ (SLC25) gehört. Bisher wurde, basierend auf der Homologie zu anderen UCPs und der vermuteten Entkopplungsaktivität an der mitochondrialen Atmungskette vorgeschlagen, dass UCP4 seine physiologische Funktion in der Regulation von ROS, der Thermogenese, sowie der der Calciumhomöostase haben könnte. Zusätzlich wird eine Beteiligung an der Zelldifferenzierung sowie dem Zelltod diskutiert. Allerdings konnte keine dieser präsentierten Funktionen in der Vergangenheit eindeutig bestätigt werden. Einige vorangegangene Studien beobachteten eine Verschiebung des Energiestoffwechsels durch UCP4 in Anpassung an äußere Bedingungen Zudem deuten auch jüngste Berichte darauf hin, dass Proteine der UCP-Familie (UCP2 und UCP3) als duale Transporter von Protonen und Substraten agieren, und ihre Expression mit dem Zellstoffwechselstatus zusammenhängt. Deshalb stellen wir die Hypothese auf, dass UCP4 für die metabolische Flexibilität von Neuronen eine wesentliche Rolle spielt.

In dieser Arbeit wollen wir überprüfen, (i) ob die Expression von UCP4 durch anhaltende Veränderungen in der Verfügbarkeit von Nährstoffen beeinflusst wird, sowie (ii) inwiefern die Menge von UCP4 Protein sich, abhängig von der unterschiedlichen anatomischen Struktur und metabolischen Aktivität, innerhalb einzelner Hirnregionen unterscheidet.

Um unsere Hypothese zu untersuchen, wurden für diese Arbeit vier verschiedene Gehirnregionen von Mäusen mit Hilfe von RT-qPCR und Western Blots analysiert, um Informationen über Veränderungen in Gen- und Proteinexpression zu erhalten. Die Mäuse wurden zuvor acht Wochen entweder (A) mit fettreichen ketogenen Diäten, die nur langkettige Fettsäuren (LCT) oder lang- und mittelkettige Fettsäuren (LCT/MCT) enthielten gefüttert. (B) Zwei weitere Gruppen wurden entweder durch intermittierendes Fasten (IF) oder eine Kalorienrestiktion (CR) gefastet.

Wir konnten feststellen, dass die UCP4 Gen- aber nicht die Proteinexpression im Hippocampus nach acht Wochen LCT/MCT gesteigert ist. Im Gegensatz dazu ließ sich im Cerebellum von CR Tieren eine geringere UCP4 Genexpression erkennen, die wiederum nicht in Veränderungen auf Proteinebene resultierte. Unter unseren Versuchsbedingungen ist demnach im Gehirn keine Korrelation zwischen den Parametern Fütterungsreglement und UCP4 Proteinexpression ersichtlich.

Allerdings ließen sich interessanterweise im Vergleich der untersuchten Hirnregionen unterschiedliche Mengen des UCP4 Proteins nachweisen, wobei der Hypothalamus die höchste Menge enthielt. Wir konnten vorangegangene Ergebnisse, die auch in Astrozyten

UCP4 Protein identifiziert haben bestätigen, wenn auch der Anteil in Astrozyten deutlich geringer war als jener in Neuronen.

Da wir mit unserem Modell keine diätbedingten Veränderungen der UCP4 Proteinexpression feststellen konnten, kann der hinlänglich bekannte, positive Einfluss diätetischer Interventionen, neurodegenerativen Krankheiten vorzubeugen und ihren Verlauf zu verzögern, höchstwahrscheinlich nicht der Funktion von UCP4 zugeordnet werden.

## 8. Abbreviations

| | |
|---|---|
| BAT | Brown adipose tissue |
| BHB | Betahydroxybutyrate |
| CACT | Carnitine-acylcarnitine-translocase |
| CPT1c | Carnitine palmitoyl transferase 1c |
| CPT2 | Carnitine palmitoyl transferase 2 |
| CR | Calorie restricted |
| ct | Cycle of quantification |
| ETC | Electron transport chain |
| FA | Fatty acid |
| FAO | Fatty acid oxidation |
| Gck | Glucokinase |
| GFAP | Glial fibrillary acidic protein |
| GLUT1, 3 | Glucose transporter 1, 3 |
| GdmCl | Guanidinhydrochlorid |
| HFD | High fatty diet |
| HKG | Housekeeping gene |
| HRP | Horseradish Peroxidase |
| IBA1 | Ionized calcium-binding adapter molecule 1 |
| IB UCP4 | UCP4 Inclusion Body |
| IF | Intermittent fasting |
| IMM | Inner mitochondrial membrane |
| KD | Ketogenic diet |
| LD | Lipid droplet |
| LCFA | Long chain fatty acids |
| LCT | Long chain triglycerides |
| MCFA | Medium chain fatty acids |

| | |
|---|---|
| MCT | Medium chain triglycerides |
| NEFA | Non-esterified fatty acid |
| NeuN | Neuronal Nuclei |
| nf-$H_2O$ | Nuclease free water |
| NTC | No template control |
| OGDH | Oxoglutarate Dehydrogenase |
| OMM | Outer mitochondrial membrane |
| OXPHOS | Oxidative phosphorylation |
| PDHC | Pyruvate dehydrogenase complex |
| PGC1a | peroxisome proliferator–activated receptor gamma coactivator 1 alpha |
| RIN | RNA integrity number |
| ROS | Reactive oxidative species |
| RPL4 | Ribosomal protein L4 |
| RT | Room temperature |
| Rt- | Reverse transcription control |
| SD | Standard diet |
| SDHA | Complex II |
| SIRT | Sirtuin |
| SOD1 | Superoxiddismutase 1 |
| TCA cycle | Tricarboxylic acid cycle |
| Tm | Melting Temperature |
| UCP | Uncoupling protein |
| UCP4 | Uncoupling protein 4 |
| VDAC | Voltage dependent anion channel |

## 9. References

Alán, L., Smolková, K., Kronusová, E., Santorová, J., & Jezek, P. (2009). Absolute levels of transcripts for mitochondrial uncoupling proteins UCP2, UCP3, UCP4, and UCP5 show different patterns in rat and mice tissues, *Journal of bioenergetics and biomembranes 41*(1) 71–78. https://doi.org/10.1007/s10863-009-9201-2

Alberts, B.,Johnson, A., Lewis, J., Morgan,D., Raff, M., Roberts, K., Walter, P.(2015). Molecular biology of the cell. Sixth Edition New York: Norton & Company

Anton, S. D., Moehl, K., Donahoo, W. T., Marosi, K., Lee, S. A., Mainous, A. G., 3rd, Leeuwenburgh, C., & Mattson, M. P. (2018). Flipping the Metabolic Switch: Understanding and Applying the Health Benefits of Fasting. *Obesity* (Silver Spring, Md.), 26(2), 254–268. https://doi.org/10.1002/oby.22065

Bélanger, M., Allaman, I., & Magistretti, P. J. (2011). Brain energy metabolism: focus on astrocyte-neuron metabolic cooperation. *Cell metabolism*, 14(6), 724–738. https://doi.org/10.1016/j.cmet.2011.08.016

Bell, A. H., Miller, S. L., Castillo-Melendez, M., & Malhotra, A. (2020). The Neurovascular Unit: Effects of Brain Insults During the Perinatal Period. *Frontiers in neuroscience*, 13, 1452. https://doi.org/10.3389/fnins.2019.01452

Bordone, M. P., Salman, M. M., Titus, H. E., Amini, E., Andersen, J. V., Chakraborti, B., Diuba, A. V., Dubouskaya, T. G., Ehrke, E., Espindola de Freitas, A., Braga de Freitas, G., Gonçalves, R. A., Gupta, D., Gupta, R., Ha, S. R., Hemming, I. A., Jaggar, M., Jakobsen, E., Kumari, P., Lakkappa, N., …, Seidenbecher, C. I. (2019). The energetic brain - A review from students to students. *Journal of neurochemistry*, 151(2), 139–165. https://doi.org/10.1111/jnc.14829

Borecký, J., Maia, I. G., & Arruda, P. (2001). Mitochondrial uncoupling proteins in mammals and plants. *Bioscience reports*, 21(2), 201–212. https://doi.org/10.1023/a:1013604526175

Bough, K. J., Wetherington, J., Hassel, B., Pare, J. F., Gawryluk, J. W., Greene, J. G., Shaw, R., Smith, Y., Geiger, J. D., & Dingledine, R. J. (2006). Mitochondrial biogenesis in the anticonvulsant mechanism of the ketogenic diet. *Annals of neurology*, 60(2), 223–235. https://doi.org/10.1002/ana.20899

Bustin, S. and Hugget, J. (2017). qPCR primer design revisited, *Biomolecular Detection and Quantification* 14, 19–28 https://doi.org/10.1016/j.bdq.2017.11.001

Ceccarelli, S. M., Chomienne, O., Gubler, M., & Arduini, A. (2011). Carnitine palmitoyltransferase (CPT) modulators: a medicinal chemistry perspective on 35 years of

research. *Journal of medicinal chemistry*, 54(9), 3109–3152. https://doi.org/10.1021/jm100809g

Cantó, C., & Auwerx, J. (2009). PGC-1alpha, SIRT1 and AMPK, an energy sensing network that controls energy expenditure. *Current opinion in lipidology,* 20(2), 98–105. https://doi.org/10.1097/MOL.0b013e328328d0a4

Cogliati, S., Enriquez, J. A., & Scorrano, L. (2016). Mitochondrial Cristae: Where Beauty Meets Functionality. *Trends in biochemical sciences*, 41(3), 261–273. https://doi.org/10.1016/j.tibs.2016.01.001

de Haas, A. H., Boddeke, H. W., & Biber, K. (2008). Region-specific expression of immunoregulatory proteins on microglia in the healthy CNS. Glia, 56(8), 888–894. https://doi.org/10.1002/glia.20663

de Jonge, H. J., Fehrmann, R. S., de Bont, E. S., Hofstra, R. M., Gerbens, F., Kamps, W. A., de Vries, E. G., van der Zee, A. G., te Meerman, G. J., & ter Elst, A. (2007). Evidence based selection of housekeeping genes, *PloS one 2*(9) e898. https://doi.org/10.1371/journal.pone.0000898

Ebert, D., Haller, R. G., & Walton, M. E. (2003). Energy contribution of octanoate to intact rat brain metabolism measured by 13C nuclear magnetic resonance spectroscopy. *The Journal of neuroscience* 23(13), 5928–5935. https://doi.org/10.1523/JNEUROSCI.23-13-05928.2003

Edmond, J., Robbins, R. A., Bergstrom, J. D., Cole, R. A., & de Vellis, J. (1987). Capacity for substrate utilization in oxidative metabolism by neurons, astrocytes, and oligodendrocytes from developing brain in primary culture. *Journal of neuroscience research*, 18(4), 551–561. https://doi.org/10.1002/jnr.490180407

Falkowska, A., Gutowska, I., Goschorska, M., Nowacki, P., Chlubek, D., & Baranowska-Bosiacka, I. (2015). Energy Metabolism of the Brain, Including the Cooperation between Astrocytes and Neurons, Especially in the Context of Glycogen Metabolism. *International journal of molecular sciences,* 16(11), 25959–25981. https://doi.org/10.3390/ijms161125939

Farmer, B. C., Walsh, A. E., Kluemper, J. C., & Johnson, L. A. (2020). Lipid Droplets in Neurodegenerative Disorders. *Frontiers in neuroscience*, 14, 742. https://doi.org/10.3389/fnins.2020.00742

Fecher, C., Trovò, L., Müller, S. A., Snaidero, N., Wettmarshausen, J., Heink, S., Ortiz, O., Wagner, I., Kühn, R., Hartmann, J., Karl, R. M., Konnerth, A., Korn, T., Wurst, W., Merkler, D., Lichtenthaler, S. F., Perocchi, F., & Misgeld, T. (2019). Cell-type-specific profiling of

brain mitochondria reveals functional and molecular diversity. *Nature neuroscience*, 22(10), 1731–1742. https://doi.org/10.1038/s41593-019-0479-z

Fernández-Vizarra, E., Enríquez, J. A., Pérez-Martos, A., Montoya, J., & Fernández-Silva, P. (2011). Tissue-specific differences in mitochondrial activity and biogenesis. *Mitochondrion*, 11(1), 207–213. https://doi.org/10.1016/j.mito.2010.09.011

Fornasiero, E. F., Mandad, S., Wildhagen, H., Alevra, M., Rammner, B., Keihani, S., Opazo, F., Urban, I., Ischebeck, T., Sakib, M. S., Fard, M. K., Kirli, K., Centeno, T. P., Vidal, R. O., Rahman, R. U., Benito, E., Fischer, A., Dennerlein, S., Rehling, P., Feussner, I., … Rizzoli, S. O. (2018). Precisely measured protein lifetimes in the mouse brain reveal differences across tissues and subcellular fractions. *Nature communications*, *9*(1), 4230. https://doi.org/10.1038/s41467-018-06519-0

Haddad-Tóvolli, R., Dragano, N., Ramalho, A., & Velloso, L. A. (2017). Development and Function of the Blood-Brain Barrier in the Context of Metabolic Control. *Frontiers in neuroscience,* 11, 224. https://doi.org/10.3389/fnins.2017.00224

Herculano-Houzel S. (2010). Coordinated scaling of cortical and cerebellar numbers of neurons. *Frontiers in neuroanatomy*, 4, 12. https://doi.org/10.3389/fnana.2010.00012

Hilse, K. E., Kalinovich, A. V., Rupprecht, A., Smorodchenko, A., Zeitz, U., Staniek, K., Erben, R. G., & Pohl, E. E. (2016). The expression of UCP3 directly correlates to UCP1 abundance in brown adipose tissue. *Biochimica et biophysica acta*, *1857*(1), 72–78. https://doi.org/10.1016/j.bbabio.2015.10.011

Hilse, K. E., Rupprecht, A., Egerbacher, M., Bardakji, S., Zimmermann, L., Wulczyn, A., & Pohl, E. E. (2018). The Expression of Uncoupling Protein 3 Coincides With the Fatty Acid Oxidation Type of Metabolism in Adult Murine Heart. *Frontiers in physiology*, *9*, 747. https://doi.org/10.3389/fphys.2018.00747

Itoh, Y., Esaki, T., Shimoji, K., Cook, M., Law, M. J., Kaufman, E., & Sokoloff, L. (2003). Dichloroacetate effects on glucose and lactate oxidation by neurons and astroglia in vitro and on glucose utilization by brain in vivo. *PNAS*, 100(8), 4879–4884. https://doi.org/10.1073/pnas.0831078100

Jensen, N. J., Wodschow, H. Z., Nilsson, M., & Rungby, J. (2020). Effects of Ketone Bodies on Brain Metabolism and Function in Neurodegenerative Diseases. *International journal of molecular sciences*, 21(22), 8767. https://doi.org/10.3390/ijms21228767

Jezek, P., & Urbánková, E. (2000). Specific sequence of motifs of mitochondrial uncoupling proteins. *IUBMB life*, 49(1), 63–70. https://doi.org/10.1080/713803586

Jezek, P., Zácková, M., Růzicka, M., Skobisová, E., & Jabůrek, M. (2004). Mitochondrial uncoupling proteins--facts and fantasies. Physiological research, 53 Suppl 1, S199–S211.

Kossoff, E. H., & Wang, H. S. (2013). Dietary therapies for epilepsy. *Biomedical journal*, 36(1), 2–8. https://doi.org/10.4103/2319-4170.107152

Lagouge, M., Argmann, C., Gerhart-Hines, Z., Meziane, H., Lerin, C., Daussin, F., Messadeq, N., Milne, J., Lambert, P., Elliott, P., Geny, B., Laakso, M., Puigserver, P., & Auwerx, J. (2006). Resveratrol improves mitochondrial function and protects against metabolic disease by activating SIRT1 and PGC-1alpha. *Cell,* 127(6), 1109–1122. https://doi.org/10.1016/j.cell.2006.11.013

Perreten Lambert, H., Zenger, M., Azarias, G., Chatton, J. Y., Magistretti, P. J., & Lengacher, S. (2014). Control of mitochondrial pH by uncoupling protein 4 in astrocytes promotes neuronal survival. *The Journal of biological chemistry*, 289(45), 31014–31028. https://doi.org/10.1074/jbc.M114.570879

Le Foll C. (2019). Hypothalamic Fatty Acids and Ketone Bodies Sensing and Role of FAT/CD36 in the Regulation of Food Intake. *Frontiers in physiology*, 10, 1036. https://doi.org/10.3389/fphys.2019.01036

Le Foll, C., & Levin, B. E. (2016). Fatty acid-induced astrocyte ketone production and the control of food intake. *American journal of physiology. Regulatory, integrative and comparative physiology*, 310(11), R1186–R1192. https://doi.org/10.1152/ajpregu.00113.2016

Longo, V. D., & Mattson, M. P. (2014). Fasting: molecular mechanisms and clinical applications. *Cell metabolism*, 19(2), 181–192. https://doi.org/10.1016/j.cmet.2013.12.008

Lin, A. L., Coman, D., Jiang, L., Rothman, D. L., & Hyder, F. (2014). Caloric restriction impedes age-related decline of mitochondrial function and neuronal activity. *Journal of cerebral blood flow and metabolism*, 34(9), 1440–1443. https://doi.org/10.1038/jcbfm.2014.114

Liu, D., Chan, S. L., de Souza-Pinto, N. C., Slevin, J. R., Wersto, R. P., Zhan, M., Mustafa, K., de Cabo, R., & Mattson, M. P. (2006). Mitochondrial UCP4 mediates an adaptive shift in energy metabolism and increases the resistance of neurons to metabolic and oxidative stress. *Neuromolecular medicine, 8*(3), 389–414. https://doi.org/10.1385/NMM:8:3:389

Magistretti, P. J., & Allaman, I. (2015). A cellular perspective on brain energy metabolism and functional imaging. *Neuron*, 86(4), 883–901. https://doi.org/10.1016/j.neuron.2015.03.035

Martin, B., Mattson, M. P., & Maudsley, S. (2006). Caloric restriction and intermittent fasting: two potential diets for successful brain aging. *Ageing research reviews*, 5(3), 332–353. https://doi.org/10.1016/j.arr.2006.04.002

Martin, E., Rosenthal, R. E., & Fiskum, G. (2005). Pyruvate dehydrogenase complex: metabolic link to ischemic brain injury and target of oxidative stress. Journal of neuroscience research, 79(1-2), 240–247. https://doi.org/10.1002/jnr.20293

Mattson, M. P., & Liu, D. (2003). Mitochondrial potassium channels and uncoupling proteins in synaptic plasticity and neuronal cell death. *Biochemical and biophysical research communications*, 304(3), 539–549. https://doi.org/10.1016/s0006-291x(03)00627-2

Maya-Monteiro, C. M., Corrêa-da-Silva, F., Hofmann, S. S., Hesselink, M., la Fleur, S. E., & Yi, C. X. (2021). Lipid Droplets Accumulate in the Hypothalamus of Mice and Humans with and without Metabolic Diseases. *Neuroendocrinology*, 111(3), 263–272. https://doi.org/10.1159/000508735

McGarry, J. D., & Foster, D. W. (1979). In support of the roles of malonyl-CoA and carnitine acyltransferase I in the regulation of hepatic fatty acid oxidation and ketogenesis. *The Journal of biological chemistry*, *254*(17), 8163–8168.

Miller, V. J., Villamena, F. A., & Volek, J. S. (2018). Nutritional Ketosis and Mitohormesis: Potential Implications for Mitochondrial Function and Human Health. *Journal of nutrition and metabolism*, *2018*, 5157645. https://doi.org/10.1155/2018/5157645

Mittelbronn, M., Dietz, K., Schluesener, H. J., & Meyermann, R. (2001). Local distribution of microglia in the normal adult human central nervous system differs by up to one order of magnitude. *Acta neuropathologica*, 101(3), 249–255. https://doi.org/10.1007/s004010000284

Mullen, R. J., Buck, C. R., & Smith, A. M. (1992). NeuN, a neuronal specific nuclear protein in vertebrates. Development (Cambridge, England), 116(1), 201–211.

Nedergaard, J., Golozoubova, V., Matthias, A., Asadi, A., Jacobsson, A., & Cannon, B. (2001). UCP1: the only protein able to mediate adaptive non-shivering thermogenesis and metabolic inefficiency. *Biochimica et biophysica acta*, 1504(1), 82–106. https://doi.org/10.1016/s0005-2728(00)00247-4

Nolfi-Donegan, D., Braganza, A., & Shiva, S. (2020). Mitochondrial electron transport chain: Oxidative phosphorylation, oxidant production, and methods of measurement. *Redox biology*, 37, 101674. https://doi.org/10.1016/j.redox.2020.101674

Owen, O. E., Morgan, A. P., Kemp, H. G., Sullivan, J. M., Herrera, M. G., & Cahill, G. F., Jr (1967). Brain metabolism during fasting. The Journal of clinical investigation, 46(10), 1589–1595. https://doi.org/10.1172/JCI105650

Palmieri F. (2004). The mitochondrial transporter family (SLC25): physiological and pathological implications. *Pflugers Archiv : European journal of physiology*, *447*(5), 689–709. https://doi.org/10.1007/s00424-003-1099-7

Perreten Lambert, H., Zenger, M., Azarias, G., Chatton, J. Y., Magistretti, P. J., & Lengacher, S. (2014). Control of mitochondrial pH by uncoupling protein 4 in astrocytes promotes neuronal survival. *The Journal of biological chemistry,* 289(45), 31014–31028. https://doi.org/10.1074/jbc.M114.570879

Pifferi, F., Laurent, B., & Plourde, M. (2021). Lipid Transport and Metabolism at the Blood-Brain Interface: Implications in Health and Disease. *Frontiers in physiology*, 12, 645646. https://doi.org/10.3389/fphys.2021.645646

Pohl, E. E., Rupprecht, A., Macher, G., & Hilse, K. E. (2019). Important Trends in UCP3 Investigation. *Frontiers in physiology*, *10*, 470. https://doi.org/10.3389/fphys.2019.00470

Popesko, P.;,Rajtová, V. and Horák, J.(2003) Anatomy of Small Laboratory Animals, Volume 2: Rat, Mouse and Hamster, Saunders Ltd

Qi, G., Mi, Y., Shi, X., Gu, H., Brinton, R. D., & Yin, F. (2021). ApoE4 Impairs Neuron-Astrocyte Coupling of Fatty Acid Metabolism. *Cell reports*, 34(1), 108572. https://doi.org/10.1016/j.celrep.2020.108572

Puchalska, P., & Crawford, P. A. (2017). Multi-dimensional Roles of Ketone Bodies in Fuel Metabolism, Signaling, and Therapeutics. *Cell metabolism*, 25(2), 262–284. https://doi.org/10.1016/j.cmet.2016.12.022

Ramsden, D. B., Ho, P. W., Ho, J. W., Liu, H. F., So, D. H., Tse, H. M., Chan, K. H., & Ho, S. L. (2012). Human neuronal uncoupling proteins 4 and 5 (UCP4 and UCP5): structural properties, regulation, and physiological role in protection against oxidative stress and mitochondrial dysfunction, *Brain and behavior* 2(4) 468–478. https://doi.org/10.1002/brb3.55

Richard, D., Rivest, R., Huang, Q., Bouillaud, F., Sanchis, D., Champigny, O., & Ricquier, D. (1998). Distribution of the uncoupling protein 2 mRNA in the mouse brain. *The Journal of comparative neurology*, 397(4), 549–560. https://doi.org/10.1002/(SICI)1096-9861(19980810)397:4<549::AID-CNE7>3.0.CO;2-1

Roberts, M. N., Wallace, M. A., Tomilov, A. A., Zhou, Z., Marcotte, G. R., Tran, D., Perez, G., Gutierrez-Casado, E., Koike, S., Knotts, T. A., Imai, D. M., Griffey, S. M., Kim, K., Hagopian, K., McMackin, M. Z., Haj, F. G., Baar, K., Cortopassi, G. A., Ramsey, J. J., & Lopez-Dominguez, J. A. (2017). A Ketogenic Diet Extends Longevity and Healthspan in Adult Mice. *Cell metabolism*, *26*(3), 539–546.e5. https://doi.org/10.1016/j.cmet.2017.08.005

Rodler, D. und Sinowatz, F.(2019)Histologie in der Tiermedizin: Grundlagen, Techniken, Präparate. First Edition. Augsburg: Schlütersche Verlagsgesellschaft

Rojas-Morales, P., Tapia, E., & Pedraza-Chaverri, J. (2016). β-Hydroxybutyrate: A signaling metabolite in starvation response?. *Cellular signalling*, 28(8), 917–923. https://doi.org/10.1016/j.cellsig.2016.04.005

Rolfe, D. F., & Brown, G. C. (1997). Cellular energy utilization and molecular origin of standard metabolic rate in mammals. *Physiological reviews*, 77(3), 731–758. https://doi.org/10.1152/physrev.1997.77.3.731

Romano, A., Koczwara, J. B., Gallelli, C. A., Vergara, D., Micioni Di Bonaventura, M. V., Gaetani, S., & Giudetti, A. M. (2017). Fats for thoughts: An update on brain fatty acid metabolism. *The international journal of biochemistry & cell biology*, 84, 40–45. https://doi.org/10.1016/j.biocel.2016.12.015

Rousset, S., Alves-Guerra, M. C., Mozo, J., Miroux, B., Cassard-Doulcier, A. M., Bouillaud, F., & Ricquier, D. (2004). The biology of mitochondrial uncoupling proteins. *Diabetes*, *53 Suppl 1*, S130–S135. https://doi.org/10.2337/diabetes.53.2007.s130

Rupprecht, A., Bräuer, A. U., Smorodchenko, A., Goyn, J., Hilse, K. E., Shabalina, I. G., Infante-Duarte, C., & Pohl, E. E. (2012). Quantification of uncoupling protein 2 reveals its main expression in immune cells and selective up-regulation during T-cell proliferation. *PloS one*, 7(8), e41406. https://doi.org/10.1371/journal.pone.0041406

Rupprecht, A., Sittner, D., Smorodchenko, A., Hilse, K. E., Goyn, J., Moldzio, R., Seiler, A. E., Bräuer, A. U., & Pohl, E. E. (2014). Uncoupling protein 2 and 4 expression pattern during stem cell differentiation provides new insight into their putative function. *PloS one*, *9*(2), e88474. https://doi.org/10.1371/journal.pone.0088474

Sanchis, D., Fleury, C., Chomiki, N., Goubern, M., Huang, Q., Neverova, M., Grégoire, F., Easlick, J., Raimbault, S., Lévi-Meyrueis, C., Miroux, B., Collins, S., Seldin, M., Richard, D., Warden, C., Bouillaud, F., & Ricquier, D. (1998). BMCP1, a novel mitochondrial carrier with high expression in the central nervous system of humans and rodents, and respiration uncoupling activity in recombinant yeast. *The Journal of biological chemistry*, 273(51), 34611–34615. https://doi.org/10.1074/jbc.273.51.34611

Saper, C. B., & Lowell, B. B. (2014). The hypothalamus. *Current biology* : CB, 24(23), R1111–R1116. https://doi.org/10.1016/j.cub.2014.10.023

Sauerbeck, A., Pandya, J., Singh, I., Bittman, K., Readnower, R., Bing, G., & Sullivan, P. (2011). Analysis of regional brain mitochondrial bioenergetics and susceptibility to mitochondrial inhibition utilizing a microplate based system. J*ournal of neuroscience methods*, 198(1), 36–43. https://doi.org/10.1016/j.jneumeth.2011.03.007

Schönfeld, P., & Reiser, G. (2013). Why does brain metabolism not favor burning of fatty acids to provide energy? Reflections on disadvantages of the use of free fatty acids as fuel for brain. *Journal of cerebral blood flow and metabolism*, 33(10), 1493–1499. https://doi.org/10.1038/jcbfm.2013.128

Schönfeld, P., & Wojtczak, L. (2016). Short- and medium-chain fatty acids in energy metabolism: the cellular perspective. *Journal of lipid research*, 57(6), 943–954. https://doi.org/10.1194/jlr.R067629

Schrauwen, P., & Hesselink, M. K. (2004). The role of uncoupling protein 3 in fatty acid metabolism: protection against lipotoxicity?. *The Proceedings of the Nutrition Society*, *63*(2), 287–292. https://doi.org/10.1079/PNS2003336

Smorodchenko, A., Rupprecht, A., Fuchs, J., Gross, J., & Pohl, E. E. (2011). Role of mitochondrial uncoupling protein 4 in rat inner ear. *Molecular and cellular neurosciences*, *47*(4), 244–253. https://doi.org/10.1016/j.mcn.2011.03.002

Smorodchenko, A., Rupprecht, A., Sarilova, I., Ninnemann, O., Bräuer, A. U., Franke, K., Schumacher, S., Techritz, S., Nitsch, R., Schuelke, M., & Pohl, E. E. (2009). Comparative analysis of uncoupling protein 4 distribution in various tissues under physiological conditions and during development. *Biochimica et biophysica acta*, *1788*(10), 2309–2319. https://doi.org/10.1016/j.bbamem.2009.07.018

Smorodchenko, A., Schneider, S., Rupprecht, A., Hilse, K., Sasgary, S., Zeitz, U., Erben, R. G., & Pohl, E. E. (2017). UCP2 up-regulation within the course of autoimmune encephalomyelitis correlates with T-lymphocyte activation. *Biochimica et biophysica acta*. Molecular basis of disease, 1863(4), 1002–1012. https://doi.org/10.1016/j.bbadis.2017.01.019

Sullivan, P. G., Rippy, N. A., Dorenbos, K., Concepcion, R. C., Agarwal, A. K., & Rho, J. M. (2004). The ketogenic diet increases mitochondrial uncoupling protein levels and activity. *Annals of neurology,* 55(4), 576–580. https://doi.org/10.1002/ana.20062

Takahashi S. (2020). Metabolic compartmentalization between astroglia and neurons in physiological and pathophysiological conditions of the neurovascular unit. Neuropathology : *official journal of the Japanese Society of Neuropathology*, 40(2), 121–137. https://doi.org/10.1111/neup.12639

Takahashi, S., Iizumi, T., Mashima, K., Abe, T., & Suzuki, N. (2014). Roles and regulation of ketogenesis in cultured astroglia and neurons under hypoxia and hypoglycemia. *ASN neuro,* 6(5), 1759091414550997. https://doi.org/10.1177/1759091414550997

Thevenet, J., De Marchi, U., Domingo, J. S., Christinat, N., Bultot, L., Lefebvre, G., Sakamoto, K., Descombes, P., Masoodi, M., & Wiederkehr, A. (2016). Medium-chain fatty

acids inhibit mitochondrial metabolism in astrocytes promoting astrocyte-neuron lactate and ketone body shuttle systems. *FASEB journal,* 30(5), 1913–1926. https://doi.org/10.1096/fj.201500182

Ventura-Clapier, R., Garnier, A., & Veksler, V. (2008). Transcriptional control of mitochondrial biogenesis: the central role of PGC-1alpha. *Cardiovascular research*, 79(2), 208–217. https://doi.org/10.1093/cvr/cvn098

Vidali, S., Aminzadeh, S., Lambert, B., Rutherford, T., Sperl, W., Kofler, B., & Feichtinger, R. G. (2015). Mitochondria: The ketogenic diet--A metabolism-based therapy. *The international journal of biochemistry & cell biology*, *63*, 55–59. https://doi.org/10.1016/j.biocel.2015.01.022

Wai, T., & Langer, T. (2016). Mitochondrial Dynamics and Metabolic Regulation. *Trends in endocrinology and metabolism*, 27(2), 105–117. https://doi.org/10.1016/j.tem.2015.12.001

Wallace, D. C., Fan, W., & Procaccio, V. (2010). Mitochondrial energetics and therapeutics. *Annual review of pathology*, 5, 297–348. https://doi.org/10.1146/annurev.pathol.4.110807.092314

Wang, Y., Liu, Z., Han, Y., Xu, J., Huang, W., & Li, Z. (2018). Medium Chain Triglycerides enhances exercise endurance through the increased mitochondrial biogenesis and metabolism. *PloS one*, *13*(2), e0191182. https://doi.org/10.1371/journal.pone.0191182

Wheless J. W. (2001). The ketogenic diet: an effective medical therapy with side effects. *Journal of child neurology*, 16(9), 633–635. https://doi.org/10.1177/088307380101600901

Wu, Y., Chen, M., & Jiang, J. (2019). Mitochondrial dysfunction in neurodegenerative diseases and drug targets via apoptotic signaling. Mitochondrion, 49, 35–45. https://doi.org/10.1016/j.mito.2019.07.003

Xu, S., Tao, H., Cao, W., Cao, L., Lin, Y., Zhao, S. M., Xu, W., Cao, J., & Zhao, J. Y. (2021). Ketogenic diets inhibit mitochondrial biogenesis and induce cardiac fibrosis. *Signal transduction and targeted therapy*, 6(1), 54. https://doi.org/10.1038/s41392-020-00411-4

Yu, X. X., Mao, W., Zhong, A., Schow, P., Brush, J., Sherwood, S. W., Adams, S. H., & Pan, G. (2000). Characterization of novel UCP5/BMCP1 isoforms and differential regulation of UCP4 and UCP5 expression through dietary or temperature manipulation. *FASEB journal : official publication of the Federation of American Societies for Experimental Biology*, 14(11), 1611–1618. https://doi.org/10.1096/fj.14.11.1611

Zhou, W., Mukherjee, P., Kiebish, M. A., Markis, W. T., Mantis, J. G., & Seyfried, T. N. (2007). The calorically restricted ketogenic diet, an effective alternative therapy for malignant brain cancer. *Nutrition & metabolism*, *4*, 5. https://doi.org/10.1186/1743-7075-4-5

https://mouse.brain-map.org/static/brainexplorer

https://www.ncbi.nlm.nih.gov/nucleotide/

https://www.ncbi.nlm.nih.gov/tools/primer-blast/

➡ Ye, J., Coulouris, G., Zaretskaya, I., Cutcutache, I., Rozen, S., & Madden, T. L. (2012). Primer-BLAST: a tool to design target-specific primers for polymerase chain reaction. BMC bioinformatics, 13, 134. https://doi.org/10.1186/1471-2105-13-134

# 10. List of Figures and Tables

## 10.1 Figures

Suppl. Fig. 5: **Representative Western Blots showing specifity of purified UCP4 antibody 2021/R2, which was used for the experiments (A)** 1µg inclusion body containing recombinant UCP4 protein and 20µg protein lysate of different brain standards as positive control and heart, spleen and liver standards as negative control were loaded on Western Blot. The blue box frames the UCP4 protein, detected by the antibody. Precision Plus Protein Dual Color Standard was used as marker. SDHA and ß-actin were used as housekeeping proteins **(B)** 1µg UCP4 inclusion body and20-40 µg protein lysate of different cells and hippocampus isolated according to 1 RIPA and 2 InnuSolv as positive control and spleen standard as negative control were loaded on Western Blot.

## 10.2 Tables

## 11. Supplement

| ***Suppl. Table 1:*** *nutrient composition of the diets* | | | | | |
|---|---|---|---|---|---|
| | **SD** | **LCT** | **LCT/MCT** | **CR** | **IF** |
| **producer** | ssniff | ssniff | ssniff | ssniff | ssniff |
| **product numbers** | S9139-E028 | S9139-E025 | S9139-E032 | V53x R/M-H auto | V53x R/M-H auto |
| **ratio fat:carbohydrates** | | 8:1 | 8:1 | | |
| | | | | | |
| **ME [MJ/kg]** | 15.1 | >29.7 | 29.7 | 12.9 | 12.9 |
| | | | | | |
| **Crude Protein %** | 16.1 | 8.1 | 8.1 | 19 | 19 |
| **Crude fiber%** | 10 | 9.9 | 9.9 | 4.9 | 4.9 |
| **Crude fat %** | 7.1 | 74.6 | 74.6 | 3.3 | 3.3 |
| **Crude ash%** | 4.5 | 4.4 | 4.4 | 6.4 | 6.4 |
| | | | | | |
| **not defined fats** | 0.1 | 0 | 0 | 0.05 | 0.05 |
| **LCT %** | 7.0 | 74.6 | 49.6 | 3.25 | 3.25 |
| **C8 %** | 0 | 0 | 15 | n.s | n.s |
| **C10 %** | 0 | 0 | 10 | n.s | n.s |
| | | | | | |
| **Sugar %** | 6 | 1 | 1 | 4.7 | 4.7 |
| **Starch %** | 51.2 | 0 | 0 | 36.5 | 36.5 |
| **NFE (total)** | n.s. | n.s. | n.s. | 54.1 | 54.1 |

n.s.: no specification

| ***Suppl. Table 2:*** *Devices* | | |
|---|---|---|
| | Application | Company |
| FastPrep-24™ | Homogenisation of brain tissue | MP Biomedicals, Germany |
| Thermomixer®R | RNA and Protein resolubilisation | Eppendorf, Germany |
| GeneAmp™ PCR System 9700 | cDNA synthesis | PE Applied Biosystems, Thermo Fisher Scientific, Austria |
| Mini- PROTEAN® Tetra handcast system | Western Blot | BioRad, Austria |
| EV231 | Power supply for Western Blot | Consort, Germany |
| epMotion 5075™ˣ | Pipetting robot for 384 well plates | Eppendorf, Germany |
| qTower³ 84 | qPCR | JenaAnalytik, Germany |
| ChemiDoc-It 600 | Western Blot chemiluminescence | UVP, United Kingdom |
| TapeStation 4200 | RNA integrity check | Agilent, Austria |
| NanoDrop™ 2000 | RNA quantification | Thermo Fisher Scientific, Austria |
| Mixer Mill 200 | Homogenisation of brain tissue | Retsch, Germany |
| Sonifier B-12 | Sonication of brain lysates | Branson Sonic Power Company, US |
| Rotina 380R | Phase separation, washing processes | Hettich, Germany |
| EnSpire 2300 Multilabel reader | Protein determination | PerkinElmer, Austria |
| Quantum | Visualization of qPCR products | Vilber, Germany |

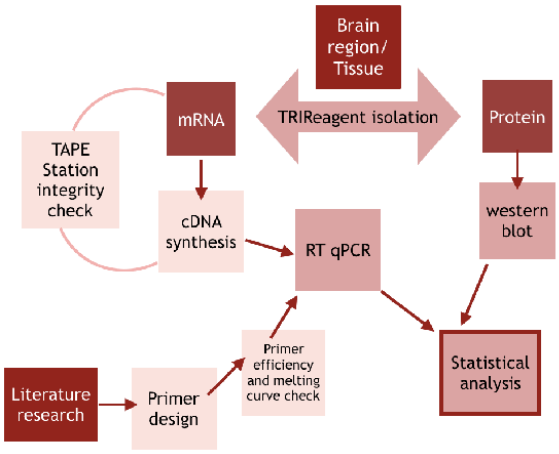


***Suppl. Figure 1: Workflow***
*Both RNA and protein were isolated from the same tissue, to compare UCP4 gene expression on one hand with its protein expression on the other hand.*

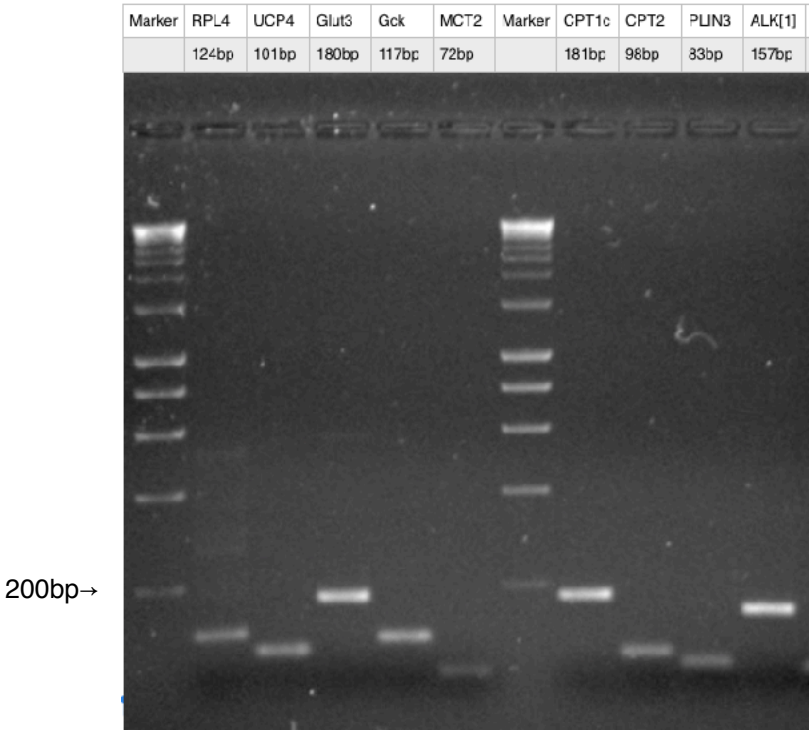


***Suppl. Figure 2: Gel electrophoresis of RT-qPCR products*** *of the primers included in first primer validation experiments. qPCR products were loaded onto an agarose gel to perform electrophoresis and afterwards visualized with UV light. Predicted sizes of the amplicons for each primer are given in the table above the gel picture. The approximate actual size of the amplicons can be estimated by comparing the height of the bands in the gel with the markers (Hyperladder) loaded in lane 1 and 7. RPL4 - ribosomal protein L4, UCP4 - uncoupling protein 4, GLUT3 - glucose transporter 3, MCT2 - monocarboxylate transporter 2, Gck - glucokinase, CPT1c - carnitine palmitoyltransferase 1c, CPT2 - carnitine palmitoyltransferase 2, ALK - anaplastic lymphoma kinase, PLIN3 - perilipin 3, bp- basepairs*

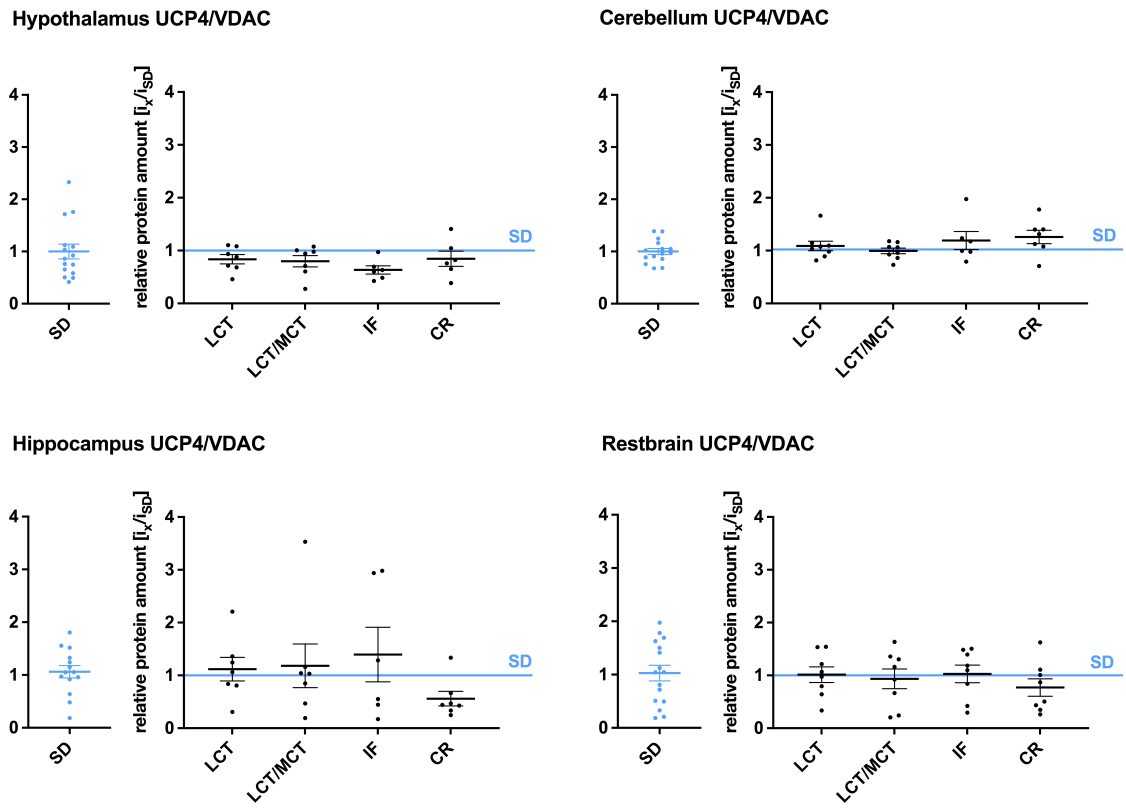


***Suppl. Figure 3: UCP4 protein expression of the different brain regions within KDs and fasting regimen***

*20µg protein lysate of eight animals per diet were loaded on Western Blot. All samples of IF and CR originated from 2019, whereas SD, LCT and LCT/MCT group include four samples from 2019 and 2021 respectively.*

*Protein levels are presented as ratios of UCP4 to VDAC($i_x$) which were detected on the same membranes consecutively and normalized towards the SD ($i_{SD}$), which was set to 1. The values are presented as mean± SEM, statistical analysis revealed no significant differences. A representative Western Blot is shown in the supplementary data.*

*SD-standard diet, LCT-long chain triglycerides, LCT/MCT-long and medium chain triglycerides, CR-caloric restriction, IF-intermitted fasting, VDAC-voltage dependent anion channel*

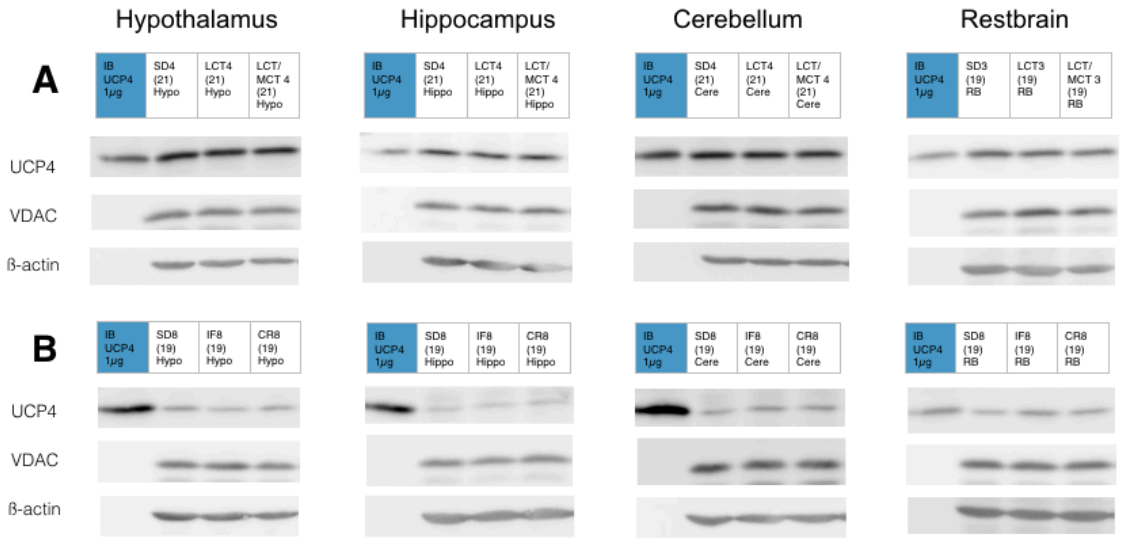


***Suppl. Figure 4: Representative Western Blots of UCP4 expression in different brain regions*** *(**A**) KDs and (**B**) fasting regimen. 20µg of tissue lysates were loaded in each lane. UCP4 inclusion body was used as a control for correct antibody binding.*
*SD-standard diet, LCT-long chain triglycerides, LCT/MCT-long and medium chain triglycerides, CR-caloric restriction, IF-intermitted fasting*

**A**

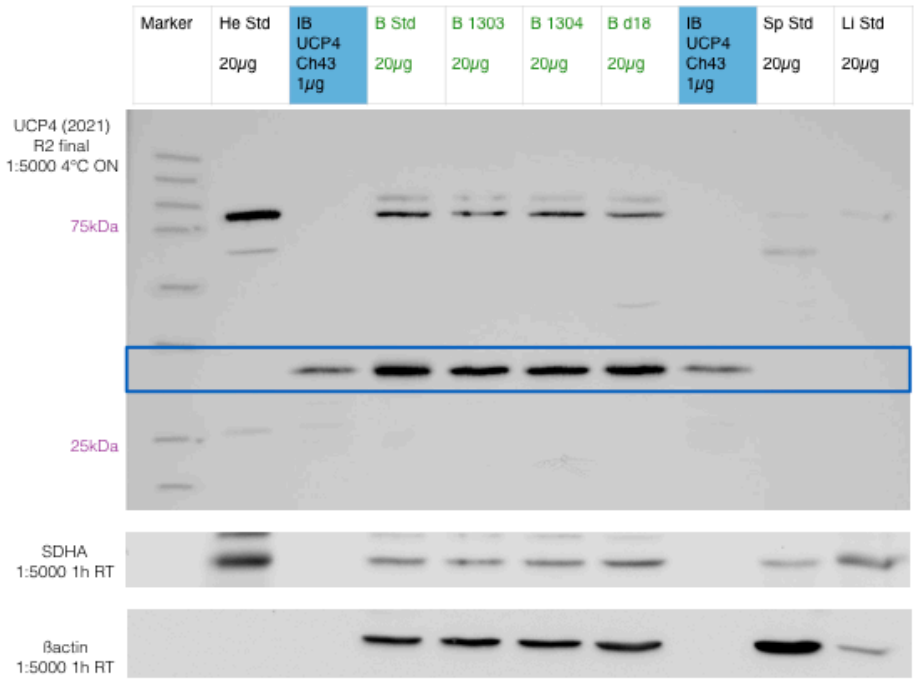


**B**

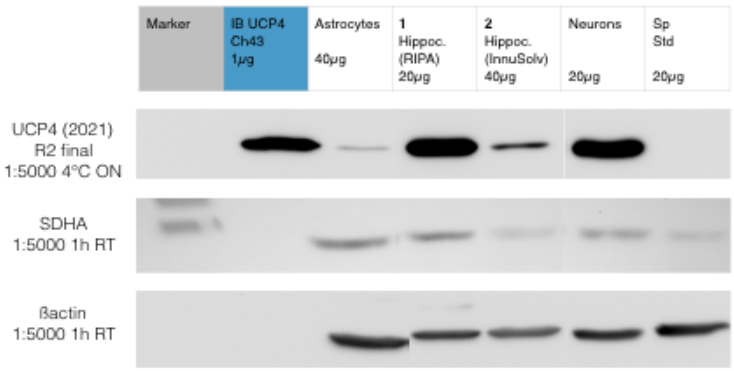


***Suppl. Figure 5: Representative Western Blots showing specifity of purified UCP4 antibody 2021/R2, which was used for the experiments***

*(**A**) 1µg inclusion body containing recombinant UCP4 protein and 20µg protein lysate of different brain standards as positive control and heart, spleen and liver standards as negative control were loaded on Western Blot. The blue box frames the UCP4 protein, detected by the antibody. Precision Plus Protein Dual Color Standard was used as marker. SDHA and ß-actin were used as housekeeping proteins*

***(B)** 1µg UCP4 inclusion body and20-40 µg protein lysate of different cells and hippocampus isolated according to 1 RIPA and 2 InnuSolv as positive control and spleen standard as negative control were loaded on Western Blot.*